ORIGINAL

W. S. Amer ⓘ

The dynamical motion of a rolling cylinder and its stability analysis: analytical and numerical investigation

Abstract The present paper addresses the dynamical motion of two degrees-of-freedom (DOF) auto-parametric system consisting of a connected rolling cylinder with a damped spring. This motion has been considered under the action of an excitation force. Lagrange's equations from second kind are utilized to obtain the governing system of motion. The uniform approximate solutions of this system are acquired up to higher order of approximation using the technique of multiple scales in view of the abolition of emerging secular terms. All resonance cases are characterized, and the primary and internal resonances are examined simultaneously to set up the corresponding modulation equations and the solvability conditions. The time histories of the amplitudes, modified phases, and the obtained solutions are graphed to illustrate the system's motion at any given time. The nonlinear stability approach of Routh–Hurwitz is used to examine the stability of the system, and the different zones of stability and instability are drawn and discussed. The characteristics of the nonlinear amplitude for the modulation equations are investigated and described, as well as their stabilities. The gained results can be considered novel and original, where the methodology was applied to a specific dynamical system.

Keywords Perturbation techniques · Nonlinear dynamics · Auto-parametric systems · Resonance · Stability · Fixed points

1 Introduction

The structure of a linked rolling cylinder with springs may be one of the important applications of the principle vibration's sources, such as in electric engines, vibrating structures, rockets, and train motors. Therefore, it is vital to completely comprehend its vibrational motion to offer a better design solution for reducing the vibration utilizing a decent plan. In this way, different sorts of frequencies and mode states of this structure are huge in the planning stage. To avoid structural familiarity, it is critical to understand where the resonance occurs.

The dynamical motions of such vibrating systems are found in many works, for example [1–10]. The spring pendulum's chaotic motion is explored in [1–3] for a fixed suspension point as in [1, 2] or a moving one in a circular path [3]. The controlling non-autonomous systems of equations of motion (EOM) are reduced to approximate autonomous systems using the technique of multiple scales (TMS) [11]. Hopf bifurcation and a series of period-doubling bifurcations [12] are demonstrated according to the existence of these systems, which lead to chaotic motions.

Many works, for example [4–9], investigate the behavior of several pendulums' types as a simple and intuitive model of a nonlinear system. The damped motion of a spring is investigated in [4] when the pivot

W. S. Amer (✉)

Department of Mathematics and Computer Science, Faculty of Science, Menoufia University, Shebin El-Koom 32511, Egypt
e-mail: drwaelamer@science.menofia.edu.eg

point follows an elliptic path, in which some special cases have been analyzed from the obtained approximate solutions, while the rigid body pendulum's motion in space is investigated numerically in [5] and [6]. The time series of the results and the corresponding diagrams of phase planes are discussed. The planar motion of an externally activated pendulum connected with a dynamic absorber that can move transversely and longitudinally is examined in [7]. The nonlinear dynamical vertical movement of a 2DOF vibrating system including nonlinear spring with nonlinear damping is studied in [8]. The analytic outcomes demonstrate that the reducing amplitude's goal and oscillation can be achieved in view of modifying the parameters of the system besides the stimulating frequency's value, whereas the motion of excited forced cart pendulum is investigated in [9]. It is noted that for dissipation with small amplitude, the hovering movements are shown to be asymptotically stable. Recently, the same problem is investigated in the framework of its approximate solution in [10], in which the authors classified and examined the arising resonances in light of the obtained modulation equations. In [13], the authors have given novel research that makes use of analytical methods to look into the nonlinear properties exhibited by diverse nonlinear events. The asymptotic method and the TMS are proven to be a practical and clear strategy for approaching mechanics and are relevant to a wide range of engineering and science domains.

The dynamics of a forced spring pendulum with viscous damping are studied in [14] and [15] under the influence of applied nonstationary restrictions that act on the point of suspension to travels in a specified path. The authors restricted the angular velocity of this point to be constant and to move along a circular trajectory [14] and a Lissajous curve [15]. A damped spring with linear and nonlinear stiffness is used to explore the motion of a linked rigid body pendulum in [16, 17] and [18, 19] to generalize the works in [4] and [15], respectively. The uniformly approximate solutions are obtained utilizing the TMS, in which three different time scales are used. The external and parametric resonance cases have been examined simultaneously.

The vibration of a sliding pendulum with clearances without considering its horizontal motion is investigated in [20]. Two models that would simulate the system's clearances with 2DOF and 3DOF are developed using nonlinear springs and dampers. Based on the obtained solutions, internal and primary resonances are studied. A controlled electromagnetic seismic damper was used to investigate the ability to dampen vibrations in a nonlinear gravitational vibratory system in [21], while the free motion of a coupled slip absorber to the motion of carrying body over a hinged roller is explored in [22].

The behavior of a nonlinear mechanical system of 3DOF double pendulum is examined in [23], in which the authors focused their study on the vibrations in the neighborhood of simultaneous internal and exterior resonances. Using the TMS, the implicit form of the resonance response functions, as well as the equations governing the modulation of amplitudes and phases, was established. Recently in [24] and [25], the authors investigated the rotatory plane motion of auto-parametric systems with 3DOF to create new vibrating dynamical motions. They comprise a primary system with a damped Duffing oscillator and a secondary one which is a damped spring pendulum. The domains of stability and instability are studied using the Routh–Hurwitz criterion [12], in which the system's behavior is found to be stable across a wide range of system's parameters.

The parametric resonances of a double pendulum exposed to vertical kinematic excitation are examined experimentally and theoretically in [26]. Theoretically, the TMS was used to generate differential equations for the slow temporal development of phases and amplitudes in the presence of parametric resonances conditions. The authors used a nonclassical strategy that included the insertion of three temporal variables proportional to the first, second, and fourth powers of a small parameter. They performed three phases of the perturbation technique corresponding to the odd powers of this parameter. The trigonometric functions are expanded around the position of stable equilibrium.

The planar motion of a nonlinear damped spring with immovable point is examined in [27]. A polynomial approximate approach is proposed in, to formulate the approximate regulating governing system of the EOM with trigonometric nonlinearities. This approach ensures that the sine and cosine functions are accurately approximated not only around a specific location, but also throughout a preset interval. The interval's size is determined in accordance with the research goals and the predicted range of the fluctuation of angle coordinate. As a result, the proposed approach could be the solution that provides improved resonance responses with geometric nonlinearities for mechanical systems. The fundamental resonance's resonant vibrations are analyzed, as well as the steady-state resonant responses. The approximate analytic solutions of a vibrating motion of a cylinder in a vertical direction are investigated in [28] using the TMS up to the second order of approximation. The stability of the fixed points at the case of steady state is examined and analyzed using the Routh–Hurwitz nonlinear stability.

In this work, the motion of a 2DOF auto-parametric dynamical system consisting of a coupled rolling cylinder with a damped spring, in which the other spring's end is connected to a wall, is examined. The
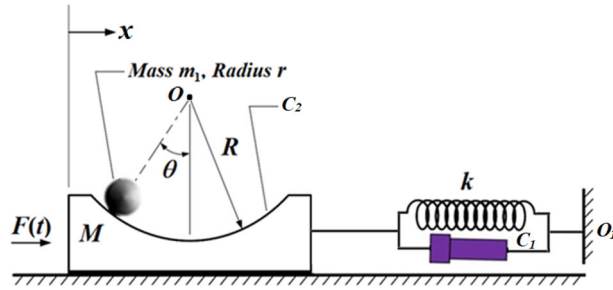
Fig. 1 The dynamical system

fundamental system of motion is derived, in the existence of an acted excited external force using Lagrange's equations of second type. This system has been solved analytically utilizing the TMS up to the third order of approximation, in which the emergent secular terms are eliminated. The solvability constraints and the equations of modulation are obtained according to the examined resonance cases. The amplitudes, adjusted phases, and acquired solutions are depicted in time histories in certain plots to show the system's motion at any instant. The emerged fixed points are examined in the steady-state case. Routh–Hurwitz's nonlinear stability strategy is utilized to investigate the system's stability, and the various areas of stabilities and instabilities are portrayed and analyzed. The nonlinear amplitudes' properties of the equations of modulation, as well as their stabilities, are explored and presented. Based on the application of used methodology on the investigated dynamical system, then we can regard the acquired results as novel and original.

2 The dynamical model

Consider the rolling motion of a cylinder with mass m_1 and radius r without slipping, on a circular surface of mass M and radius R with friction damping coefficient C_2 between the circular surface and the cylinder [29]. The system of these masses is attached with a damped linear elastic spring, of stiffness k and a damping coefficient C_1, in which the spring's other end is connected to a fixed point O_1 as seen in Fig. 1.

Let g denote the earth's gravitational acceleration, x and θ be the displacement on the x direction and the rotation angle at the center O of the circular surface. The motion is forced by an external excitation harmonic force $F(t) = F_1 \cos(\Omega_1 t)$ along x horizontal direction, in which Ω_1 and F_1 are the frequency and amplitude of the force F, respectively. The motion is considered for a rolling cylinder without slip, in which the fraction between the sliding block and the ground is neglected.

Based on the preceding explanation of the dynamical system, the kinetic and potential energies T and V can be formulated as follows

$$T = \frac{1}{2}m_1 v^2 + \frac{1}{2}M \dot{x}^2 + \frac{1}{4}m_1(R-r)^2\dot{\theta}^2,$$
$$V = \frac{1}{2}k x^2 + m_1 g(R-r)(1-cos\theta), \tag{1}$$

where the derivatives are considered concerning t.

The regulating EOM can be obtained utilizing the next Lagrange's equations

$$\frac{\mathrm{d}}{\mathrm{d}t}\left(\frac{\partial L}{\partial \dot{x}}\right) - \left(\frac{\partial L}{\partial x}\right) = F_1 \cos(\Omega_1 t) - C_1\dot{x},$$
$$\frac{\mathrm{d}}{\mathrm{d}t}\left(\frac{\partial L}{\partial \dot{\theta}}\right) - \left(\frac{\partial L}{\partial \theta}\right) = -C_2\dot{\theta}, \tag{2}$$

where $L = T - V$ is known by the Lagrangian. It must be noted that, for the viscous effects of damping and rotation, it is assumed that the friction forces have the terms $-C_1\dot{x}$ and $-C_2\dot{\theta}$, respectively.

Take a look at the below list of dimensionless parameters.

$$J = (M + m_1), \quad I = (R - r), \quad u = \frac{x}{I}, \quad \omega_1^2 = \frac{k}{J}, \quad \tilde{d} = \frac{m_1 I}{J}, \quad \omega_2^2 = \frac{2g}{3I},$$

$$s = \frac{1}{2}m_1 I, \quad m = \frac{m_1}{J}, \quad \tilde{f}_1 = \frac{F_1}{I\,J}, \quad \tilde{h} = \frac{2s}{3I}, \quad \tilde{c}_1 = \frac{C_1}{I\,J}, \quad \tilde{c}_2 = \frac{2C_2}{3m_1 I^2}. \tag{3}$$

Therefore, the dimensionless forms of the EOM can be obtained by the substitution of (1) and (3) into (2) as follows

$$\ddot{u} + \omega_1^2 u + \tilde{d}\,\ddot{\theta}\cos\theta - s\,\dot{\theta}^2\sin\theta = \tilde{f}_1\,\cos(\Omega_1 t) - \tilde{c}_1\dot{u}$$
$$\ddot{\theta} + \omega_2^2\,\sin\theta + \tilde{h}\,\ddot{u}\cos\theta = -\tilde{c}_2\dot{\theta}. \tag{4}$$

The previous system of Eqs. (4) composing two second-order nonlinear differential equations.

3 The used methodology

The major aim of this section is to derive the analytic approximate solutions of the governing system (4) utilizing the TMS up to the third order of approximation with a high degree of accuracy, and to investigate the various resonance circumstances [30]. To achieve this aim, we employ Taylor expansion to represent the functions $\sin\theta$ and $\cos\theta$ in expansion forms till the third order, which are valid in the nearness of static equilibrium's positions. As a result, Eqs. (4) can be expressed as

$$\ddot{u} + \omega_1^2 u - \frac{1}{2}\tilde{d}(\theta^2 - 2)\ddot{\theta} + \frac{1}{6}s\,\theta\dot{\theta}^2(\theta^2 - 6) = \tilde{f}_1\,\cos(\Omega_1 t) - \tilde{c}_1\dot{u},$$
$$\ddot{\theta} + \omega_2^2\theta - \frac{\tilde{h}}{2}(\theta^2 - 2)\ddot{u} - \omega_2^2\frac{\theta^3}{6} = -\tilde{c}_2\dot{\theta}. \tag{5}$$

Now, using the new variables ξ and ϕ to express the generalized coordinates u and θ as follows

$$u(\tau) = \varepsilon\,\xi(\tau;\varepsilon), \quad \theta(\tau) = \varepsilon\,\phi(\tau;\varepsilon), \tag{6}$$

where $0 < \varepsilon << 1$ is a small parameter. Based on the TMS, one can look to the approximate solutions of the variables ξ and ϕ as follows

$$\xi = \sum_{k=1}^{3}\varepsilon^k\xi_k(\tau_0,\,\tau_1,\,\tau_2) + O(\varepsilon^4),$$

$$\phi = \sum_{k=1}^{3}\varepsilon^k\phi_k(\tau_0,\,\tau_1,\,\tau_2) + O(\varepsilon^4). \tag{7}$$

Here $\tau_n = \varepsilon^n t$ ($n = 0,\,1,\,2$) represent the various time scales, where τ_0 is the fast one, while τ_1 and τ_2 are the slow scales.

To deal with these scales, the following operators are used to modify the derivatives relative to t into other ones relative to these scales

$$\frac{d}{dt} = \frac{\partial}{\partial\tau_0} + \varepsilon\frac{\partial}{\partial\tau_1} + \varepsilon^2\frac{\partial}{\partial\tau_2},$$
$$\frac{d^2}{dt^2} = \frac{\partial^2}{\partial\tau_0^2} + 2\varepsilon\frac{\partial^2}{\partial\tau_0\partial\tau_1} + \varepsilon^2\left(\frac{\partial^2}{\partial\tau_1^2} + 2\frac{\partial^2}{\partial\tau_0\partial\tau_2}\right) + O(\varepsilon^3). \tag{8}$$

Terms of $O(\varepsilon^3)$ and higher are discarded due to the smallness of ε. The generalized forces, coefficients of damping, and the related mass parameters are considered to be small. Then, we will be able to write

$$\tilde{f}_1 = \varepsilon^3\,f_1, \quad \tilde{c}_1 = \varepsilon^2\,c_1, \quad \tilde{c}_2 = \varepsilon^2\,c_2, \quad \tilde{d} = \varepsilon d, \quad \tilde{h} = \varepsilon h. \tag{9}$$

Substituting (6)–(9) in (5) and then equalling the coefficients of similar powers of ε, then one can obtain easily the below groups of partial differential equations (PDE).

Coefficient of (ε)

$$\frac{\partial^2\xi_1}{\partial\tau_0^2} + \omega_1^2\xi_1 = 0. \tag{10}$$

$$\frac{\partial^2 \phi_1}{\partial \tau_0^2} + \omega_2^2 \phi_1 = 0. \tag{11}$$

Coefficient of (ε^2)

$$\frac{\partial^2 \xi_2}{\partial \tau_0^2} + \omega_1^2 \xi_2 = -2\frac{\partial^2 \xi_1}{\partial \tau_0 \partial \tau_1} - d\frac{\partial^2 \phi_1}{\partial \tau_0^2}, \tag{12}$$

$$\frac{\partial^2 \phi_2}{\partial \tau_0^2} + \omega_2^2 \phi_2 = -2\frac{\partial^2 \phi_1}{\partial \tau_0 \tau_1} + h\frac{\partial^2 \xi_1}{\partial \tau_0^2}. \tag{13}$$

Coefficient of (ε^3)

$$\frac{\partial^2 \xi_3}{\partial \tau_0^2} + \omega_1^2 \xi_3 = f_1 \cos \Omega_1 \tau_0 - \frac{\partial^2 \xi_1}{\partial \tau_1^2} + \phi_1 \left(\frac{\partial \phi_1}{\partial \tau_0}\right)^2 - c_1 \frac{\partial \xi_1}{\partial \tau_0} - 2\frac{\partial^2 \xi_1}{\partial \tau_0 \partial \tau_2}$$

$$+ 2d\frac{\partial^2 \phi_1}{\partial \tau_0 \partial \tau_1} - 2\frac{\partial^2 \xi_2}{\partial \tau_0 \partial \tau_2} + d\frac{\partial^2 \phi_2}{\partial \tau_0^2}, \tag{14}$$

$$\frac{\partial^2 \phi_3}{\partial \tau_0^2} + \omega_2^2 \phi_3 = \frac{1}{6}\omega_2^2 \phi_1^3 - \frac{\partial^2 \phi_1}{\partial \tau_1^2} - 2\left(\frac{\partial^2 \phi_1}{\partial \tau_0 \partial \tau_2} + \frac{\partial^2 \phi_2}{\partial \tau_0 \partial \tau_1}\right)$$

$$+ 2h\frac{\partial^2 \xi_1}{\partial \tau_0 \partial \tau_1} - c_2\frac{\partial \phi_1}{\partial \tau_0} + h\frac{\partial^2 \xi_2}{\partial \tau_0^2}. \tag{15}$$

It is interesting to note that the equations of the previous systems (10)–(15) can be solved one by one. To accomplish this, we will proceed with the general solutions of (10) and (11) as follows

$$\xi_1 = A_1 e^{i\omega_1 \tau_0} + \overline{A}_1 e^{-i\omega_1 \tau_0}. \tag{16}$$

$$\phi_1 = A_2 e^{i\omega_2 \tau_0} + \overline{A}_2 e^{-i\omega_2 \tau_0}, \tag{17}$$

where A_j ($j = 1, 2$) denote the undetermined complex functions of τ_j, while $\overline{A}_j$ representing their complex conjugate.

The substitution of the solutions (16) and (17) in Eqs. (12) and (13) produces secular terms. The required conditions for removing these terms have the forms

$$\frac{\partial A_1}{\partial \tau_1} = 0, \quad \frac{\partial A_2}{\partial \tau_1} = 0, \tag{18}$$

which means that A_j are functions of τ_2 only.

As a result, the second-order solutions become

$$\xi_2 = -\frac{\omega_2^2 d A_2}{\omega_1^2 - \omega_2^2} e^{i\omega_2 \tau_0} + CC, \tag{19}$$

$$\phi_2 = -\frac{\omega_1 h A_1}{\omega_2^2 - \omega_1^2} e^{i\omega_1 \tau_0} + CC, \tag{20}$$

where CC denote the complex conjugates of the previous terms.

According to the above procedure, the third approximation necessitates the elimination of terms that produce secular ones. Therefore, the following conditions are obtained

$$\frac{h \omega_1^4 A_1}{(\omega_2^2 - \omega_1^2)} - 2i\omega_1(c_1 A_1 + \frac{\partial A_1}{\partial \tau_2}) = 0, \tag{21}$$

$$2A_2^2 \overline{A}_2 \omega_2^2 - 2i\omega_2(\frac{\partial A_2}{\partial \tau_2} + c_2 A_2) + \frac{h d\omega_2^2 A_2}{(\omega_1^2 - \omega_2^2)} = 0. \tag{22}$$

Henceforth, the third-order solutions of Eqs. (14) and (15) have the forms

$$\xi_3 = \frac{f_1 e^{i\Omega_1 \tau_0}}{2(\omega_1^2 - \Omega_1^2)} + \frac{2\omega_2^2 \overline{A}_2 A_2^2 e^{i\omega_2 \tau_0}}{\omega_1^2 - \omega_2^2} - \frac{\omega_2^2 A_2^3 e^{3i\omega_2 \tau_0}}{\omega_1^2 - 9\omega_2^2} + CC, \tag{23}$$

$$\phi_3 = -\frac{A_2^3}{48} e^{3 i \omega_2 \tau_0} + CC. \tag{24}$$

The functions A_j ($j = 1, 2$) may be determined by using the criterion of deleting secular terms (18), (21), and (22).

Based on the above approximate solutions, one can obtain and categorize the emerging cases of resonance when the dominators of these solutions tend to zero [31] as follows:

The system comes to external (primary) resonance when $\Omega_1 \approx \omega_1$ is satisfied, while we can discover the internal resonance occurs at $\omega_1 \approx \omega_2$. It should be emphasized that when any of these resonances is realized, the dynamical behavior of the system can be challenging. On the other hand, the achieved solutions are valid when the vibrations deviate from resonances.

4 Conditions of solvability

This section presents the stability of the investigated dynamical system when the resonance cases of external and internal are satisfied simultaneously in accordance with the system's solvability criteria and the equations of modulation. Based on the previous analysis of the end part of the above section, the external resonance and the internal one occurs when $\Omega_1 \approx \omega_1$ and $\omega_1 \approx \omega_2$, respectively. This means that Ω_1 and ω_1 are very near to ω_1 and ω_2, respectively. Therefore, the detuning parameters σ_j ($j = 1, 2$) can be introduced according to

$$\begin{aligned} \Omega_1 &= \omega_1 + \sigma_1, \\ \omega_1 &= \omega_2 + \sigma_2. \end{aligned} \tag{25}$$

These parameters may be regarded as a measure of the vibrations from the strict resonance [32]. Consequently, we can express them in terms of ε as follows

$$\sigma_j = \varepsilon \tilde{\sigma}_j \quad (j = 1, 2). \tag{26}$$

Substitute (25) and (26) in Eqs. (12)–(15) and pay attention to the secular terms, then eliminating these terms to gain the criteria of solvability for the second and third orders of approximation.

– For the 2nd order of approximation

$$\frac{\partial A_1}{\partial \tau_1} = 0, \qquad \frac{\partial A_2}{\partial \tau_1} = 0. \tag{27}$$

– For the 3rd approximation

$$\begin{aligned} &\frac{1}{2} f_1 e^{i\tau_1 \tilde{\sigma}_1} - 2 i \omega_1 (c_1 A_1 + \frac{\partial A_1}{\partial \tau_2}) - \frac{h\omega_1^4 A_1}{\omega_2^2 - \omega_1^2} = 0, \\ &2 \omega_2^2 A_2^2 \overline{A}_2 - 2i\omega_2(\frac{\partial A_2}{\partial \tau_2} + c_2 A_2) + 2 i \frac{h \omega_1 A_1}{\omega_2^2 - \omega_1^2} - \frac{h d \omega_2^4 A_2}{\omega_1^2 - \omega_2^2} = 0. \end{aligned} \tag{28}$$

Based on the above illustration, we can see that the conditions of solvability have four nonlinear PDE with respect to the unknown functions A_j. It is worthy to mention that these functions are only affected by the scale τ_2, as indicated from conditions (27). In the form of polar notation, we can express these functions as follows

$$A_j = \frac{\tilde{a}_j(\tau_2)}{2} e^{i\tilde{\psi}_j \tau_2}, \quad a_j = \varepsilon \tilde{a}_j \quad (j = 1, 2), \tag{29}$$

where $\tilde{\psi}_j$ and $\tilde{a}_j$ are real functions of the phases and amplitudes, respectively, of the solutions ξ and ϕ.

Referring to dependency of A_j on τ_2, we can write

$$\frac{\partial A_j}{\partial \tau} = \varepsilon^2 \frac{\partial A_j}{\partial \tau_2} \quad (j = 1, 2). \tag{30}$$

Based on these conditions, Eqs. (28) may be converted into ordinary differential equations (ODE) using the modified phases listed below [33]

$$\begin{aligned} \gamma_1(\tau_1, \tau_2) &= \tau_1 \tilde{\sigma}_1 - \psi_1(\tau_2), \\ \gamma_2(\tau_1, \tau_2) &= \tau_1 \tilde{\sigma}_2 - \psi_2(\tau_2). \end{aligned} \tag{31}$$
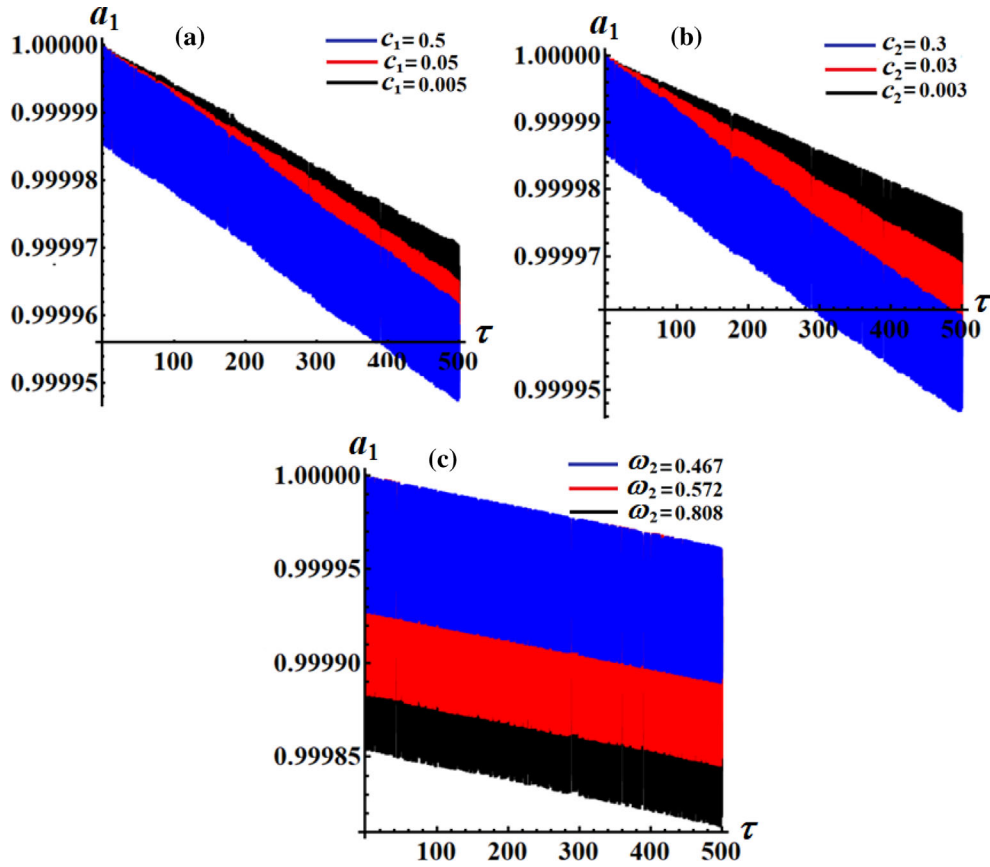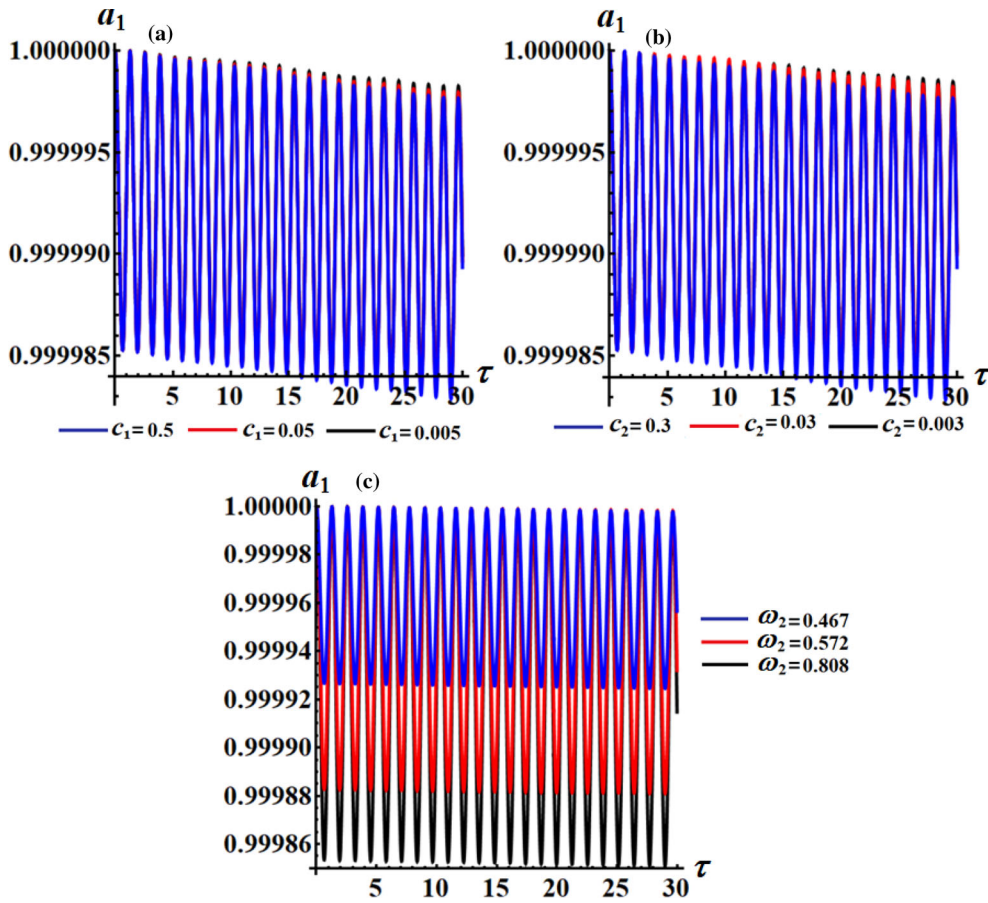
Fig. 2 The time dependency of $a_1(\tau)$; $\tau \in [0, 500]$: **a** when $c_1 = (0.5, 0.05, 0.005)$, **b** at $c_2 = (0.3, 0.03, 0.003)$, **c** when $\omega_2 = (0.467, 0.572, 0.808)$

Substitute (29)–(31) into (28) and then distinguishing the real and imaginary portions to obtain directly the following autonomous system of four first-order ODE

$$
\begin{aligned}
a_1 \frac{d\gamma_1}{d\tau} &= \frac{f_1}{2\omega_1} \cos \gamma_1 + a_1 \sigma_1 - \frac{h \, a_1 \omega_1^4}{2\omega_1(\omega_2^2 - \omega_1^2)}, \\
\frac{da_1}{d\tau} &= \frac{f_1}{2\omega_1} \sin \gamma_1 - \frac{a_1 c_1}{2}, \\
a_2 \frac{d\gamma_2}{d\tau} &= a_2 \sigma_2 - \frac{\omega_2 a_2^3}{4} - \frac{h \, d \, \omega_2^3 \, a_2}{\omega_1^2 - \omega_2^2} - \frac{h \, a_1 \, \cos \gamma_2}{\omega_2}, \\
\frac{da_2}{d\tau} &= -\frac{h \, a_1 \, sin\gamma_2}{\omega_2} - \frac{a_2 c_2}{2}.
\end{aligned}
\tag{32}
$$

The solutions of this system a_j and γ_j describe the modulation of the amplitudes and phases regarding to the dimensionless time τ when the examined resonances under study occur simultaneously. These solutions are depicted graphically in Figs. 2, 3, 4 and 5 taking into considerations the values $f = 10^{-3}$, $c_1 = 0.05$, $c_2 = 0.03$, $\sigma_1 = 0.005$, and $\sigma_2 = 0.01$.

It would be interesting to further investigation of the curves included in parts of Fig. 2. These parts represent the change in $a_1(\tau)$ at $\tau \in [0, 500]$ when $c_1(= 0.5, 0.05, 0.005)$, $c_2 = (0.3, 0.03, 0.003)$, and $\omega_2 = (0.467, 0.572, 0.808)$ as seen in portions (a), (b), and (c), respectively. These graphs have decay behaviors with the change of time till the time interval is completed. Curves of Fig. 3 show the same variation of the amplitude a_1 with time but with a small range of the time interval, i.e., at $\tau \in [0, 30]$. The reason is to go back to see the nature of the curves' oscillations as in Fig. 3 and to give an induction about these oscillations for a large time scale as graphed in Fig. 2.
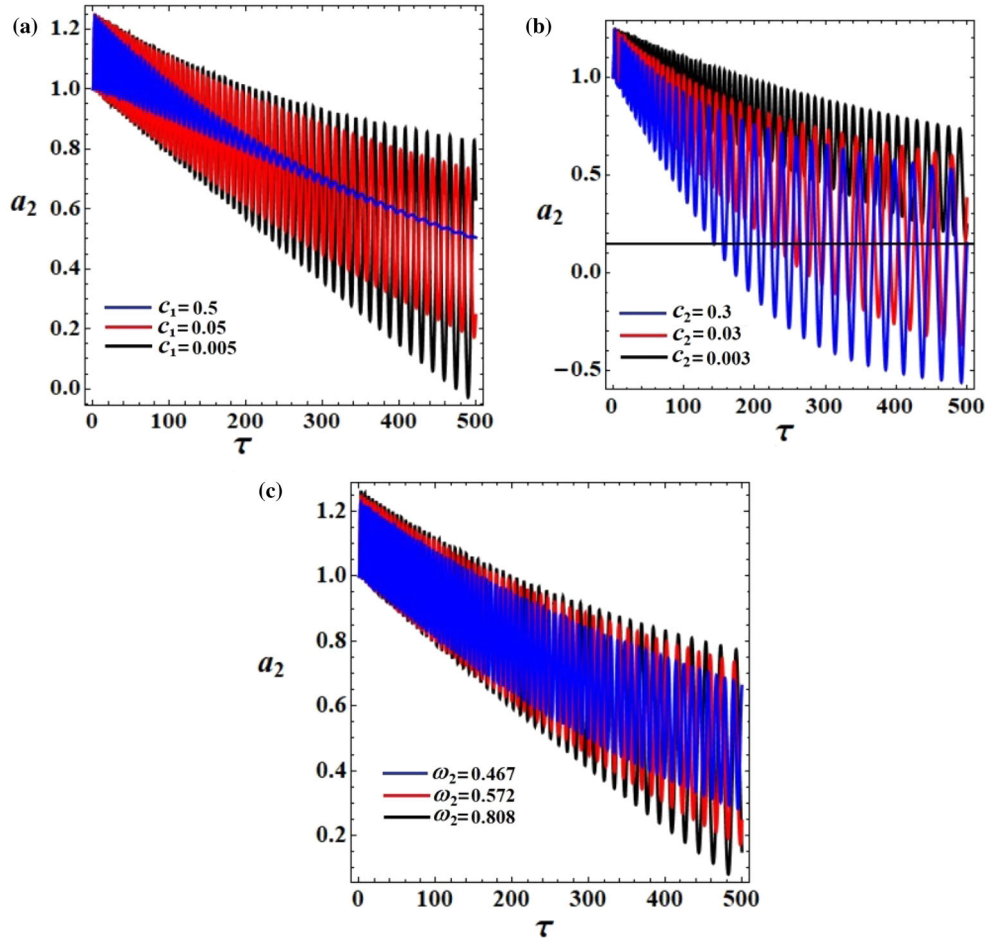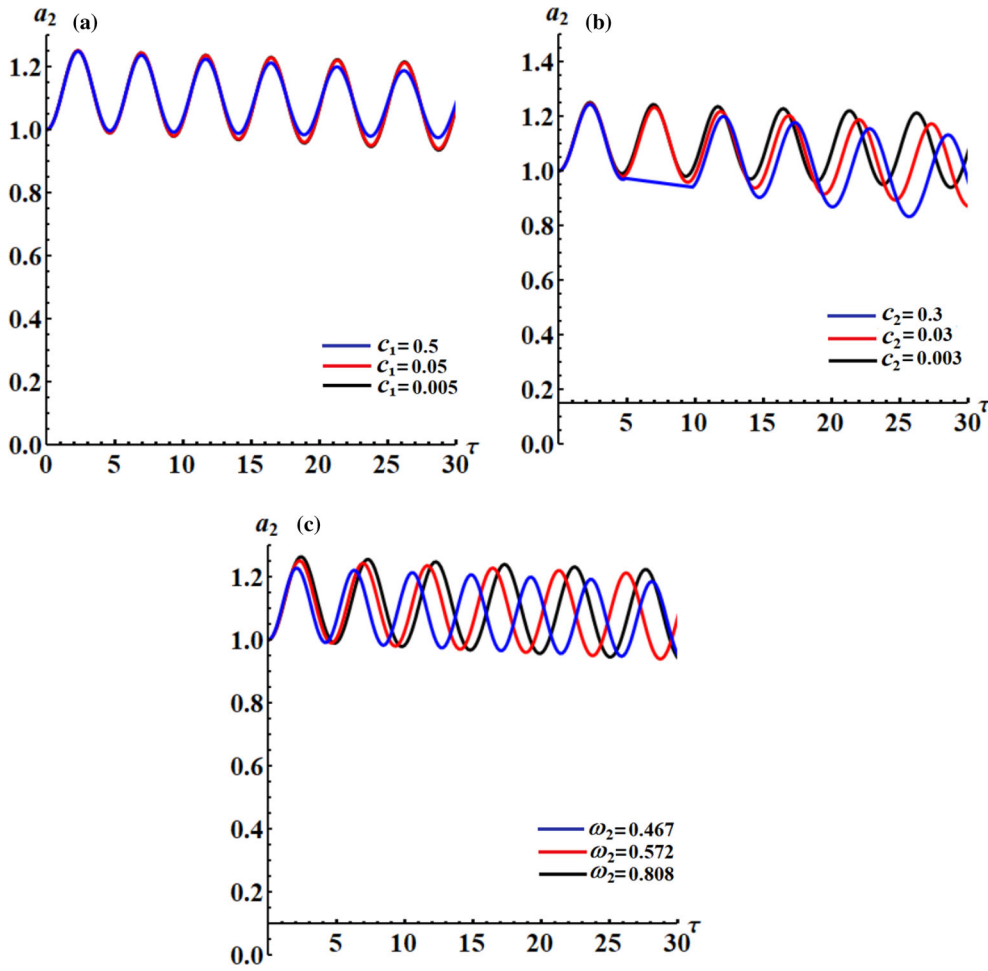
Fig. 3 The time dependency of $a_1(\tau)$; $\tau \in [0, 30]$: **a** when $c_1 = (0.5, 0.05, 0.005)$, **b** at $c_2 = (0.3, 0.03, 0.003)$, **c** when $\omega_2 = (0.467, 0.572, 0.808)$

The temporal histories of the amplitude a_2 and the phases γ_1 and γ_2 are drawn in parts of Figs. 4, 6, and 7 when $\tau \in [0, 500]$. Figure 5 shows the same variation of the amplitude a_2 with time but with a small range of the time interval, i.e., at $\tau \in [0, 30]$. The previously concluded remarks are satisfied for the plotted curves in parts of Fig. 4. Alternatively, the time variation of γ_1 and γ_2 increases and decreases with time as seen in curves of Figs. 6 and 7, respectively.

These notes are consistent with the equations of system (32), in which the good effect for the variation of the damping parameters and frequencies on the amplitudes and their corresponding phases is evident from drawn curves in these figures.

A closer inspection of the curves of Figs. 8, 9, 10 and 11 reveals the variation of the obtained approximate solutions of the springe's elongation u and the rotating angle θ with time when $\tau \in [0, 500]$ as drawn in Figs. 8 and 10, and $\tau \in [0, 30]$ as graphed in Figs. 9 and 11. These figures have been calculated in acoordance with the used parameter previously when c_1, c_2, and ω_2 have different values. The behavior of the presented solutions has decay procedures with the variation of the mentioned parameters previously. Therefore, the dynamical motion is stable during the time frame under consideration. Moreover, the amplitudes of the waves increase with the increase in c_1 and c_2 values as depicted in portions (a) and (b) of these figures, while this variation decreases when ω_2 increases as graphed in parts (c) of Figs. 10 and 11.

To confirm the employed perturbation approach is accurate, the numerical solutions (NS) regarding the original system are gained utilizing the Runge–Kutta method from the fourth order and compared with the approximate solutions (AS). This comparison is graphed in parts of Fig. 12 to demonstrate their high consistency, revealing the high reliability of the derived analytic approximate solutions. The phase diagrams when $\tau \in [0, 500]$ for $a_1(\gamma_1)$ and $a_2(\gamma_2)$ are plotted in Figs. 13 and 15, respectively.

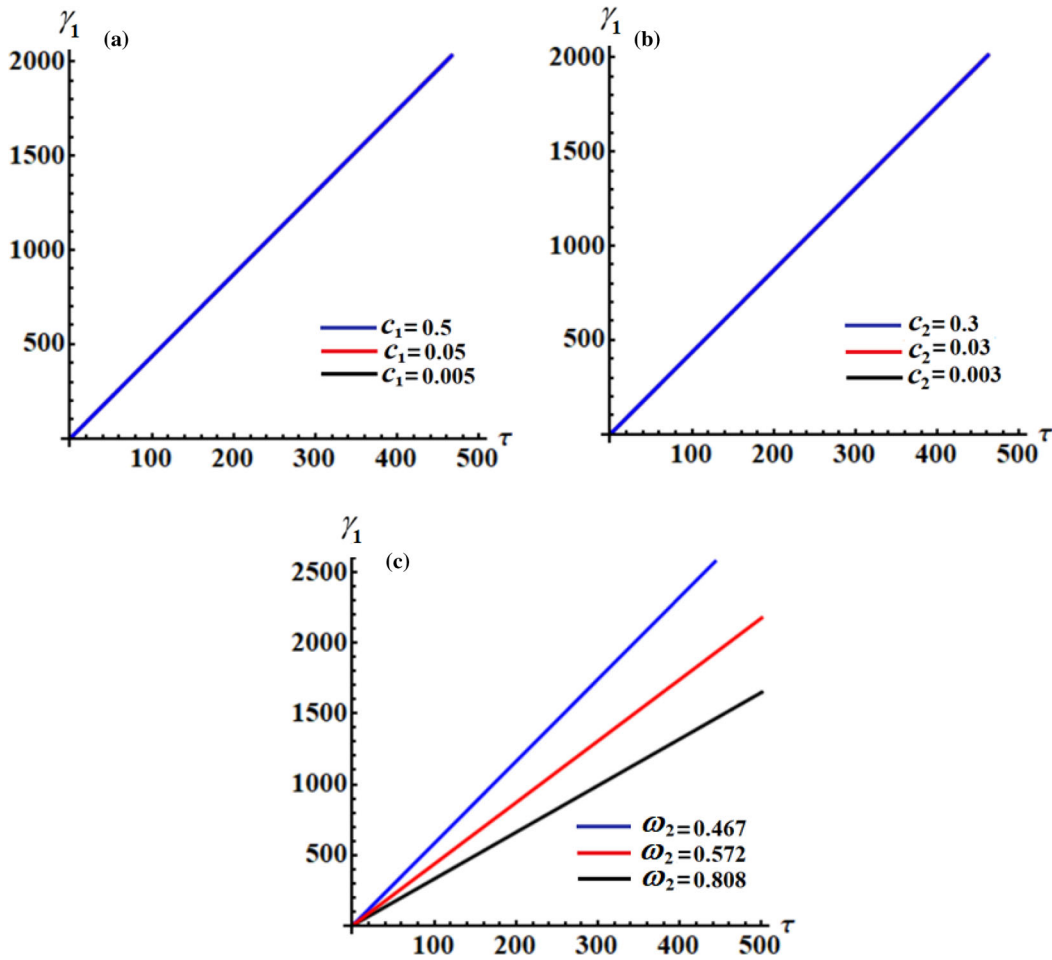**Fig. 4** The time dependency of $a_2(\tau)$; $\tau \in [0, 500]$: **a** when $c_1 = (0.5, 0.05, 0.005)$, **b** at $c_2 = (0.3, 0.03, 0.003)$, **c** when $\omega_2 = (0.467, 0.572, 0.808)$

5 Steady-state solutions

This section's main purpose is to look at the model's steady-state vibrations, in which the vibrations of the transient process vanish due to the system's damping. In such instances, the zero derivatives of the adjusted phases γ_j $(j = 1, 2)$ and the amplitudes a_j are used to determine the steady-state conditions [34]. Therefore, the system of Eqs. (32) is quite useful in characterizing them. Then, we consider $\frac{d\gamma_j}{dt} = \frac{da_j}{dt} = 0$ to getting the following algebraic equations

$$
\begin{aligned}
&\frac{f_1}{2\omega_1} \cos \gamma_1 + a_1 \sigma_1 - \frac{h\, a_1 \omega_1^4}{2\omega_1(\omega_2^2 - \omega_1^2)} = 0, \\
&\frac{f_1}{2\omega_1} \sin \gamma_1 - \frac{a_1 c_1}{2} = 0, \\
&a_2 \sigma_2 - \frac{\omega_2 a_2^3}{4} - \frac{h\, d\, \omega_2^3 a_2}{\omega_1^2 - \omega_2^2} - \frac{h\, a_1 \cos \gamma_2}{\omega_2} = 0, \\
&\frac{h\, a_1 \sin \gamma_2}{\omega_2} + \frac{a_2 c_2}{2} = 0.
\end{aligned}
\tag{33}
$$

Fig. 5 The time dependency of $a_2(\tau)$; $\tau \in [0, 30]$: **a** when $c_1 = (0.5, 0.05, 0.005)$, **b** at $c_2 = (0.3, 0.03, 0.003)$, **c** when $\omega_2 = (0.467, 0.572, 0.808)$

If we can get rid of γ_j, the below equations in terms of a_j and σ_j can be obtained

$$\frac{1}{2\omega_1^2} f_1^2 = \left(a_1\sigma_1 - \frac{h\, a_1\, \omega_1^4}{2\omega_1(\omega_2^2 - \omega_1^2)}\right)^2 + \frac{1}{4} c_1^2 a_1^2,$$

$$\frac{h^2\, a_1^2}{(\omega_2^2 - \omega_1^2)^2} = \left(a_2\sigma_2 - \frac{\omega_2 a_2^3}{4} - \frac{h\, d\, \omega_2 a_2^3}{\omega_1^2 - \omega_2^2}\right)^2 + \frac{1}{4} c_2^2 a_2^2. \tag{34}$$

It is worthy to note that the assessment of the stability analysis of the studied system includes steady-state vibrations. Therefore, we examine the system's behavior in a region relatively near to the location of the fixed points. Then we consider the substitutions [35]

$$a_1 = a_{10} + a_{11}, \qquad a_2 = a_{20} + a_{21},$$

$$\gamma_1 = \gamma_{10} + \gamma_{11}, \qquad \gamma_2 = \gamma_{20} + \gamma_{21}. \tag{35}$$

Fig. 6 The time dependency of $\gamma_1(\tau)$; $\tau \in [0, 500]$: **a** when $c_1 = (0.5, 0.05, 0.005)$, **b** at $c_2 = (0.3, 0.03, 0.003)$, **c** when $\omega_2 = (0.467, 0.572, 0.808)$

Here a_{j0} $(j = 1, 2)$ and γ_{j0} represent the unperturbed steady-state solution, whereas a_{j1} and γ_{j1} are the corresponding small perturbations. Making use of (35) into (32) to obtain the below linearized system, we get

$$
\begin{aligned}
a_{10}\frac{d\gamma_{11}}{d\tau} &= \frac{f_1}{2\omega_1}\sin\gamma_{10}\gamma_{11} + a_{11}\sigma_1 - \frac{h\,a_{11}\omega_1^4}{2\omega_1(\omega_2^2 - \omega_1^2)}, \\
\frac{da_{11}}{d\tau} &= \frac{f_1}{2\omega_1}\cos\gamma_{10}\gamma_{11} - \frac{a_{11}c_1}{2}, \\
a_{20}\frac{d\gamma_{21}}{d\tau} &= a_{21}\sigma_2 - \frac{3\omega_2 a_{20}^3 a_{21}}{4} - \frac{h\,d\,\omega_2^3\,a_{21}}{\omega_1^2 - \omega_2^2} - \frac{h}{\omega_2}(a_{10}\sin\gamma_{20}\gamma_{21} + a_{11}\cos\gamma_{20}), \\
\frac{da_{21}}{d\tau} &= -\frac{h}{\omega_2}(a_{10}\cos\gamma_{20}\gamma_{21} + a_{11}\sin\gamma_{20}) - \frac{a_{21}c_2}{2}.
\end{aligned}
\tag{36}
$$

Based on the definitions of the small perturbation a_{j1} and γ_{j1}, one can formulate their solutions as a linear combination of $k_s\,e^{\lambda\tau}$ $(s = 1, 2, 3, 4)$ in which k_s are constants and λ is the eigenvalue of these perturbations. The roots' real parts of the below characteristic equation ought to be negative if the solutions a_{j0} and γ_{j0} are stable asymptotically [36]

$$
\lambda^4 + \Gamma_1\lambda^3 + \Gamma_2\lambda^2 + \Gamma_3\lambda + \Gamma_4 = 0,
\tag{37}
$$
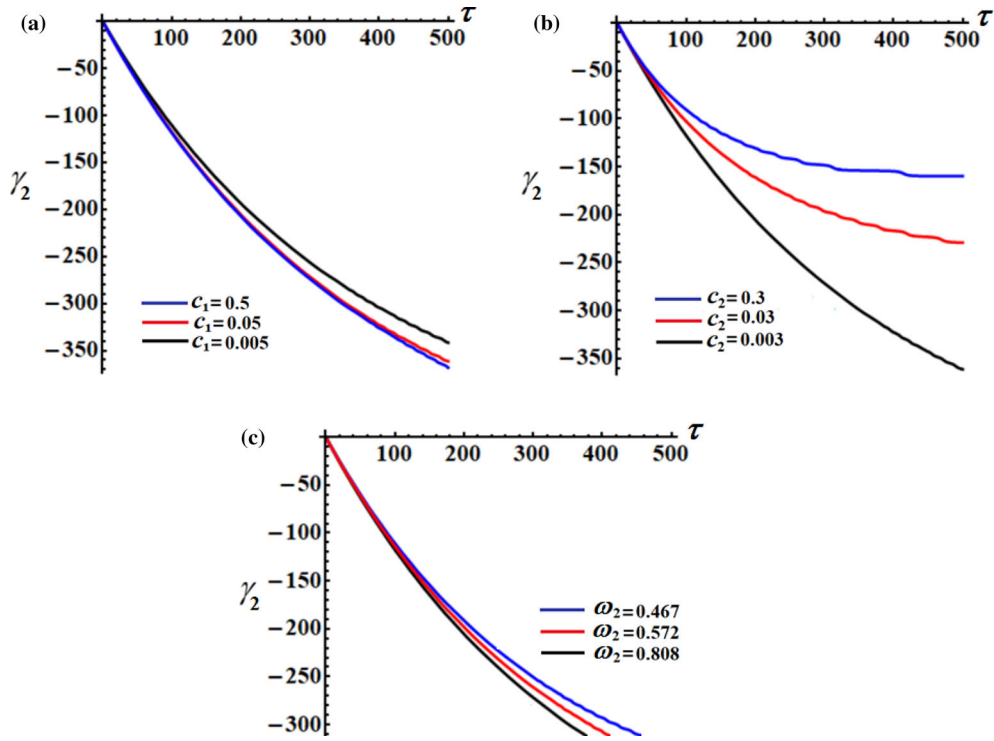
Fig. 7 The time dependency of $\gamma_2(\tau)$; $\tau \in [0, 500]$: **a** when $c_1 = (0.5, 0.05, 0.005)$, **b** at $c_2 = (0.3, 0.03, 0.003)$, **c** when $\omega_2 = (0.467, 0.572, 0.808)$

where Γ_s $(s = 1, 2, 3, 4)$ have the forms

$$\Gamma_1 = \frac{1}{2}(c_1 + c_2) - \frac{f_1}{2\,a_{10}\omega_1}\sin\gamma_{10} + \frac{h\,a_{10}}{a_{20}\omega_2}\sin\gamma_{20},$$

$$\Gamma_2 = \frac{c_1 c_2}{4} - \left(\frac{3}{4}ha_{20} + \frac{d\,h^2\omega_2^2}{2a_{20}}\right)a_{10}\cos\gamma_{20}$$
$$- \frac{(c_1 + c_2)}{4\,a_{10}\omega_1}f_1\sin\gamma_{10} + \frac{1}{2}\left[\frac{ha_{10}c_2}{a_{20}\omega_2} - \frac{f_1}{\omega_1}\left(c_1 + \frac{h\sin\gamma_{10}}{a_{10}\,\omega_2}\right)\right]\sin\gamma_{20}$$
$$+ \left[\frac{h\,a_{10}\sigma_2}{a_{20}\omega_1} - \frac{f_1}{a_{10}}\left(\frac{h\,\omega_1^2}{4} + \frac{\sigma_1}{4\,\omega_1}\right)\right]\cos\gamma_{10},$$

$$\Gamma_3 = \left[\left(3\,h\,a_{20} - \frac{4\,h\sigma_2}{a_{20}\omega_2}\right)\cos\gamma_{20} + \frac{c_1 c_2}{a_{10}\omega_1}\right]\frac{f_1}{8\,\omega_1}\sin\gamma_{10} + \left(\frac{c_1\sigma_2}{2\,a_{20}\omega_2} - \frac{d\omega_2^2 c_1}{4\,a_{20}} - \frac{3}{8}a_{20}c_1\right)$$
$$\times ha_{10}\cos\gamma_{20} + \left(\frac{2c_1\sigma_1}{\omega_1} - h\,\omega_1^2 c_2\right)\frac{f_1}{8a_{10}}\cos\gamma_{10} + \left(\frac{a_{10}c_1}{4\,a_{20}} - \frac{f_1\sin\gamma_{10}}{4\,a_{10}\omega_1}\right)\frac{h\,c_2}{\omega_2}\sin\gamma_{20}$$
$$+ \frac{df_1h^2\omega_2^2}{4\,a_{20}\omega_1}\cos\gamma_{20}\sin\gamma_{10} + \left(\frac{2\sigma_2}{a_{10}\omega_1} - \frac{h\,\omega_1^2}{a_{20}}\right)\frac{f_1 h}{4\omega_2}\cos\gamma_{10}\sin\gamma_{20},$$

$$\Gamma_4 = \left(\frac{3}{4}a_{20} - \frac{\sigma_2}{a_{20}\omega_2}\right)\frac{f_1 hc_1}{4\omega_1}\cos\gamma_{20}\sin\gamma_{10} - \left(\frac{3\,\sigma_1 a_{20}}{8\,\omega_1} - \frac{h\,c_2\omega_1^2}{4\,a_{20}\omega_2}\right)f_1 h\cos\gamma_{10}\sin\gamma_{20}$$
$$+ \left(\frac{\sigma_1}{\omega_1}\cos\gamma_{10} - c_1\sin\gamma_{10}\right)\frac{f_1 h\,c_2}{4\,a_{20}\omega_2}\sin\gamma_{20} + \frac{f_1 d\,h^2}{8\,a_{20}\omega_1}c_1\omega_2^2\cos\gamma_{20}\sin\gamma_{10} + \left(\frac{h\sigma_2}{2\omega_2}\right.$$
$$\left. - \frac{1}{4}dh^2\omega_2^2\right)\frac{\sigma_1 f_1}{\omega_1 a_{20}}\cos\gamma_{10}\sin\gamma_{10} + \left(dh\omega_2^2 + \frac{3a_{10}}{2a_{20}} - \frac{2\sigma_2}{4\omega_2}\right)\frac{h^2 f_1\omega_1^2}{8a_{20}}\cos\gamma_{10}\cos\gamma_{20}. \tag{38}$$
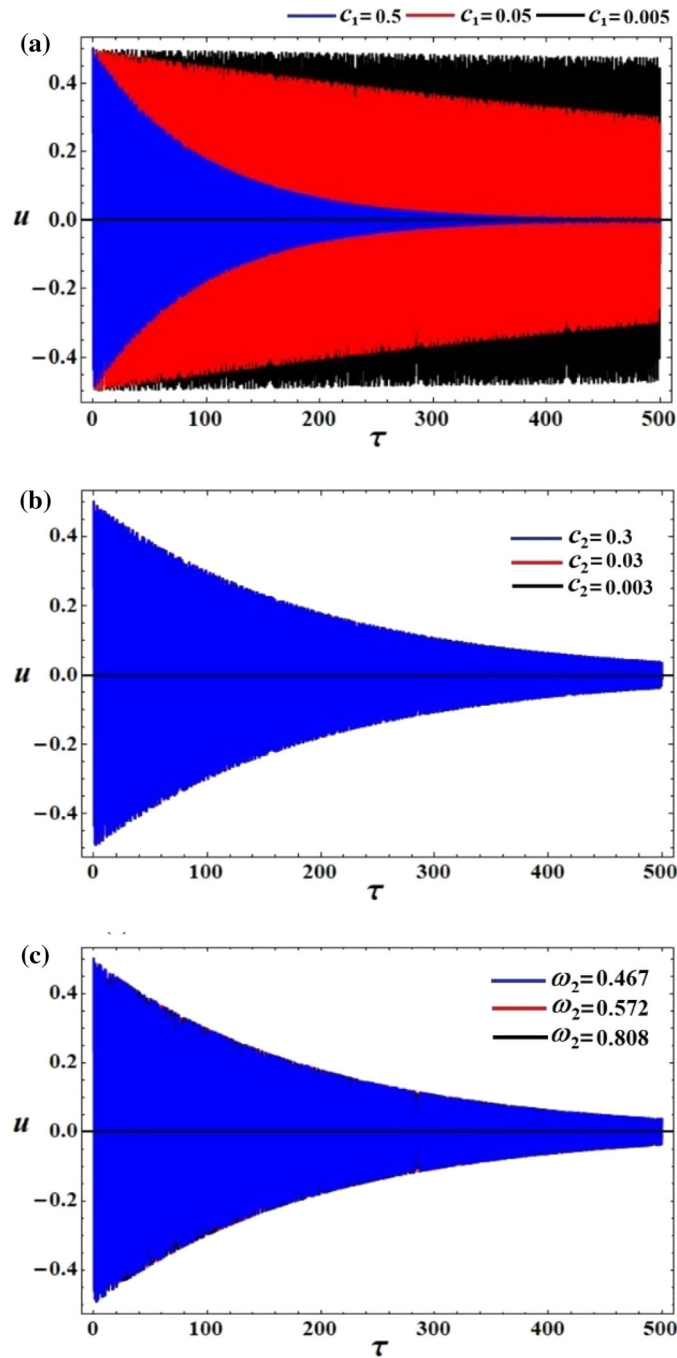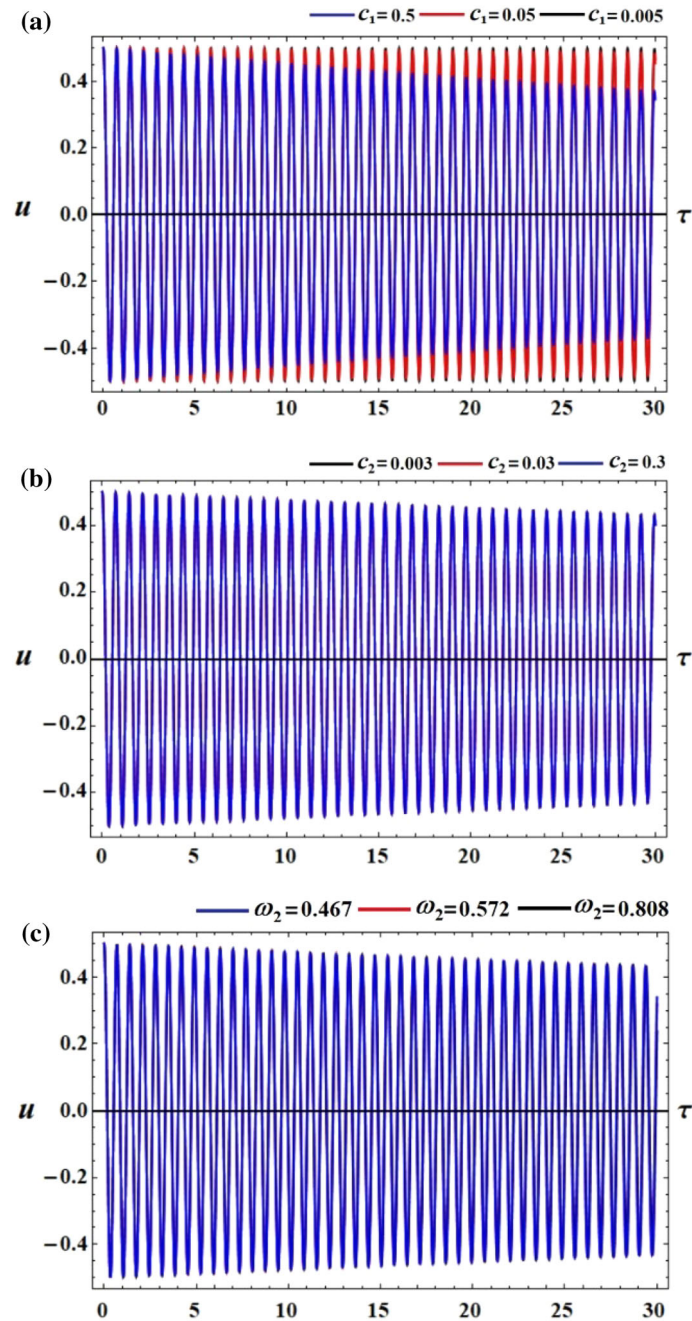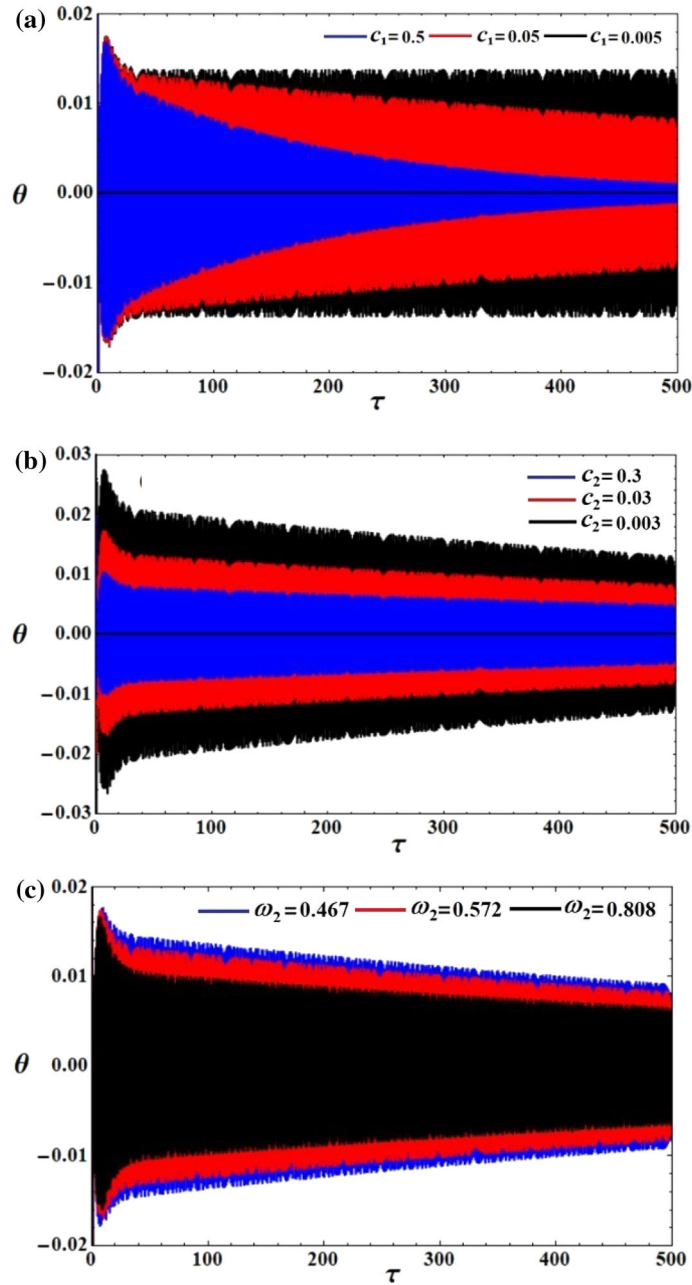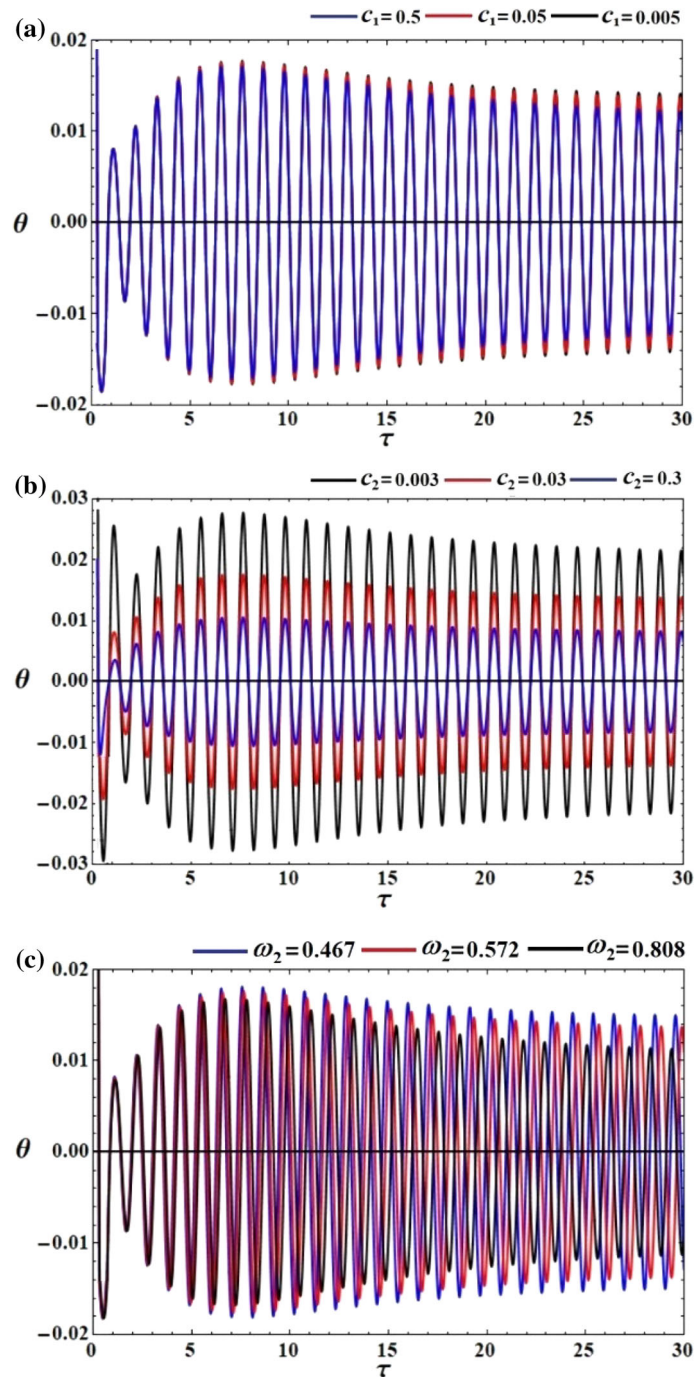
Fig. 8 The time behavior of the solution u at $\tau \in [0, 500]$: **a** when $c_1 = (0.5, 0.05, 0.005)$, **b** at $c_2 = (0.3, 0.03, 0.003)$, and **c** when $\omega_2 = (0.467, 0.572, 0.808)$

Now, we may formulate the basic conditions of the stability for specific steady-state solutions in the forms that agree with the criteria of Routh–Hurwitz [12] as follows

$$
\begin{aligned}
&\Gamma_1 > 0, \\
&\Gamma_1\Gamma_2 - \Gamma_3 > 0, \\
&\Gamma_3(\Gamma_1\Gamma_2 - \Gamma_3) - \Gamma_4\Gamma_1^2 > 0, \\
&\Gamma_4 > 0.
\end{aligned}
\tag{39}
$$

Fig. 9 The time behavior of the solution u at $\tau \in [0, 30]$: **a** when $c_1 = (0.5, 0.05, 0.005)$, **b** at $c_2 = (0.3, 0.03, 0.003)$, and **c** when $\omega_2 = (0.467, 0.572, 0.808)$

The stability analysis of the fixed points is tested in the framework of the solutions at the steady state taking into account the requirements of Routh–Hurwitz through various graphs of Eq. (34). The results are displayed in Figs. 16, 17, 18 and 19 to show the variation of a_2 versus a_1 for different values of c_1, c_2, and ω_2, in which these figures are plotted based on the following data

$$c_1 (= 0.5, 0.05, 0.005), \ c_2 (= 0.3, 0.03, 0.003), \ \varepsilon = 0.005,$$
$$f_1 = 0.001, \ \omega_2 (= 0.808, 0.572, 0.467), \ \sigma_1 = 0.02, \ \sigma_2 = 0.02.$$

The intersections of the curves of these graphs give rise to so-called fixed points, as before, which define the solutions of the equations of the system (34). These points firmly determine the axial amplitudes and the

Fig. 10 The time behavior of the solution θ at $\tau \in [0, 500]$: **a** when $c_1 = (0.5, 0.05, 0.005)$, **b** at $c_2 = (0.3, 0.03, 0.003)$, and **c** when $\omega_2 = (0.467, 0.572, 0.808)$

adjusted steady-state vibration. Furthermore, vibrations in the steady state might be either stable or not. Small pink circles indicate the stable fixed points, in which conditions (39) are satisfied, while the gray circles express the unstable ones. An inspection of these figures shows that four fixed points are obtained when $c_1 = 0.5$, $\omega_2 = 0.467$ and $c_2 = 0.3$ as seen in Fig. 16; three of them are unstable; and the latter point is stable. On the other hand, Fig. 17 is calculated according to the same previous data at $c_1 = 0.05$, $\omega_2 = 0.467$, and $c_2 = 0.3$ to yield two fixed points, and one of them is stable. To get a better overview of these points, let's examine the plotted curves in Figs. 18 and 19 which are drawn at $(c_2 = 0.03, c_1 = 0.5$ and $\omega_2 = 0.467)$ and $(\omega_2 = 0.572, c_1 = 0.5$ and $c_2 = 0.3)$, respectively. Two fixed points were achieved, one stable and the other is unstable.

Fig. 11 The time behavior of the solution u at $\tau \in [0, 30]$: **a** when $c_1 = (0.5, 0.05, 0.005)$, **b** at $c_2 = (0.3, 0.03, 0.003)$, and **c** when $\omega_2 = (0.467, 0.572, 0.808)$

Now, we are going to examine the stability of the investigated dynamical system applying the Routh–Hurwitz nonlinear stability criteria. Some parameters like the coefficients of damping c_1, c_2, the frequency ω_1, and the parameters of detuning σ_1, σ_2 play principal roles in the process of stabilization of this system. Specific operations with various parameters of the system are performed to gain the stability diagram of the system (32). The phase plane paths are used to depict the attributes of the adjusted amplitudes a_1 and a_2, which are created over time in distinct parameter domains.
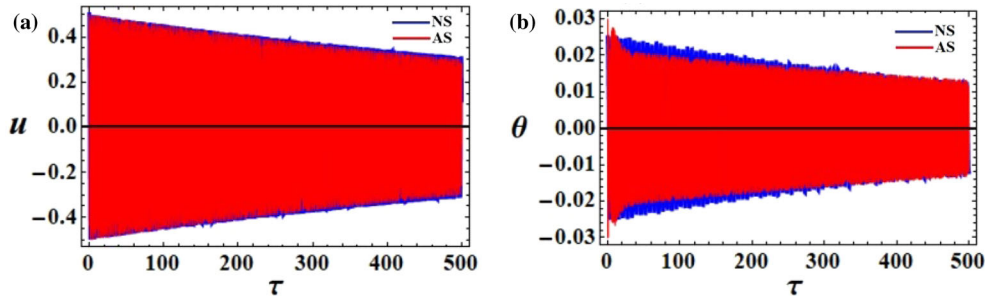
Fig. 12 The deviation between the AS and the NS at $\omega_2 = 0.808$: **a** regarding the solution u, **b** regarding the solution θ
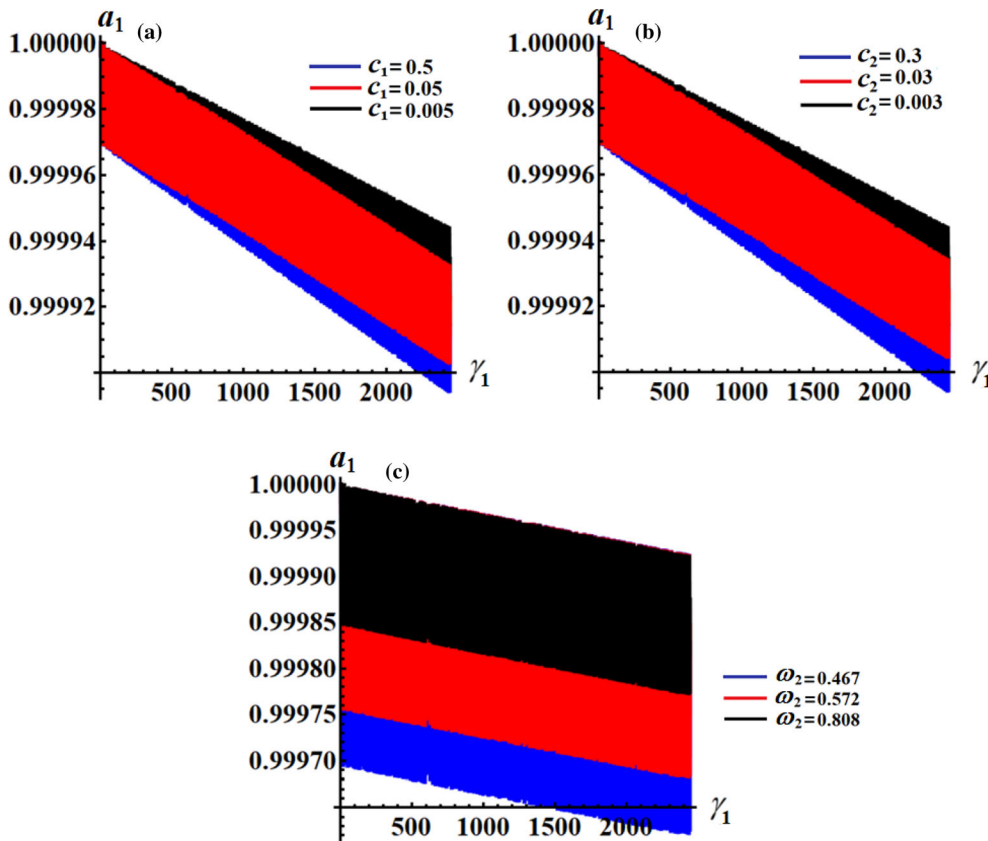
Fig. 13 The variation of the amplitude a_1 via its corresponding phase γ_1: **a** when $c_1 = (0.5, 0.05, 0.005)$, **b** at $c_2 = (0.3, 0.03, 0.003)$, **c** when $\omega_2 = (0.467, 0.572, 0.808)$ at $\tau \in [0, 500]$

Variations of feasible fixed points on different detuning parameters σ_1 are shown in Figs. 20, 21, 22, 23, 24, 25 and 26. Parts (a) and (b) of these figures show the response curves for the variation of the amplitudes a_1 and a_2 via detuning parameter σ_1, respectively. They are drawn according to the following data

$$c_1(= 0.5, 0.05, 0.005), \quad c_2(= 0.2, 0.02, 0.002), \quad \varepsilon = 0.005,$$
$$f_1 = 0.001, \quad \omega_2(= 0.808, 0.572, 0.467), \quad \sigma_2 = 0.01.$$

The inspection of the parts of Fig. 21 reveals that they are graphed at $c_1 = 0.5$ and $\omega_2 = 0.808$, in which the system was discovered to contain only one fixed point independent on the value of σ_2 over the whole domain. In this region $-1 \le \sigma_1 \le 0.05$, the fixed point is stable, whereas in $0.05 < \sigma_1 \le 1$ it is unstable. Moreover, the stable fixed points for the response curves at $c_1 = 0.05$ and $c_1 = 0.005$ are found in Figs. 21 and 22 at the domains of $-1 \le \sigma_1 \le 0.01$ and $-1 \le \sigma_1 \le 0$, respectively, when $\omega_2 = 0.808$, whereas the unstable ones exist in the zones $0.01 < \sigma_1 \le 1$ and $0 < \sigma_1 \le 1$.
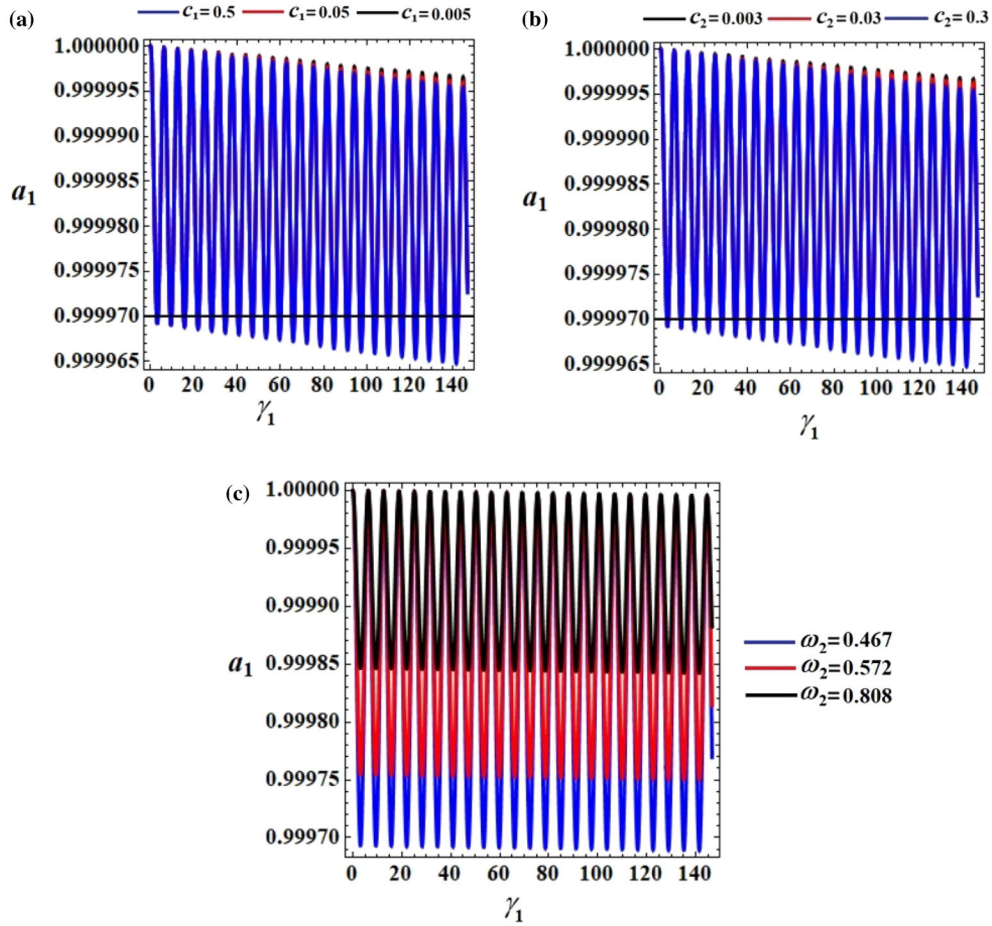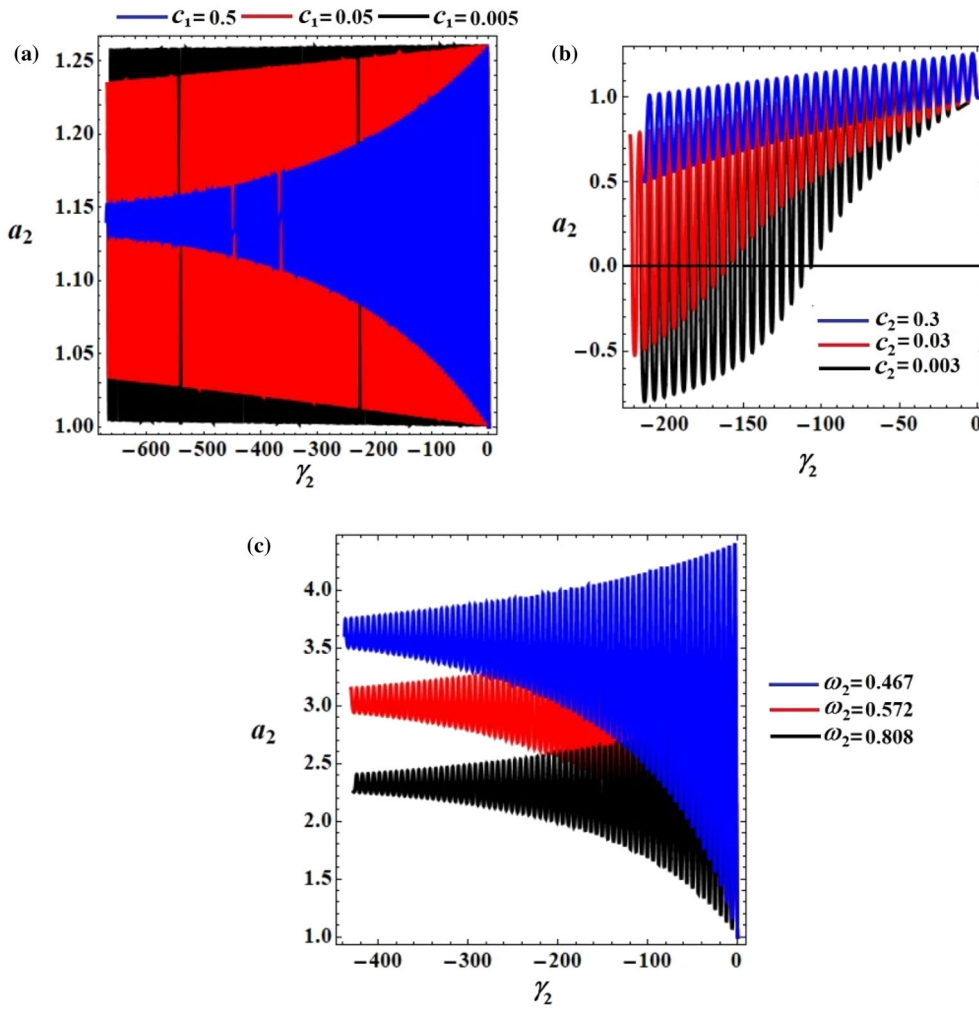
Fig. 14 The variation of the amplitude a_1 via its corresponding phase γ_1: **a** when $c_1 = (0.5, 0.05, 0.005)$, **b** at $c_2 = (0.3, 0.03, 0.003)$, **c** when $\omega_2 = (0.467, 0.572, 0.808)$ at $\tau \in [0, 30]$

The good impact of various values of c_2 and ω_2 on the curves of frequency response is observed in Figs. 23, 24 and 25, 26, respectively. Also, the influence of the detuning parameter σ_2 on the curve of frequency response is shown in Fig. 27, in which the solid curves express the region of stable fixed point and the dashed ones represent the unstable fixed region. These numbers show that the system still has a fixed point, which suggests a transcritical bifurcation of the system. This implies that when the parameters change, the system mode does not have any qualitative behavior.

Finally, Figs. 28, 29 and 30 show the projection of the modulation equations trajectories on the planes uu' and $\theta\theta'$, in which they are drawn when $c_1 = (0.5, 0.05, 0.005), c_2 = (0.3, 0.03, 0.003)$, and $\omega_2 = (0.467, 0.572, 0.808)$, respectively. For these values of the parameters, different closed curves are obtained which means that the considered system's motion is steady and chaotic-free.

To show the characteristics of the nonlinear amplitude of Eq. (32) and to analyze their stability, we will start with the next transformation [37]

$$A_1 = (p_1 + i\,q_1)e^{i\,\sigma_1\tau_2}, \qquad A_2 = (p_2 + i\,q_2)e^{i\,\sigma_2\tau_2}. \tag{40}$$

Making use of (40) into (32), then separate the real and imaginary components to get

$$2\omega_1 q_1' = \frac{h\,\omega_1^4}{\omega_2^2 - \omega_1^2}p_1 - 2\omega_1 p_1\sigma_1 - 2c_1\omega_1 q_1 - \frac{f_1}{2},$$

$$2\omega_1 p_1' = 2\omega_1 q_1\sigma_1 - \frac{h\,\omega_1^4}{\omega_2^2 - \omega_1^2}q_1 - 2c_1\omega_1 p_1,$$

Fig. 15 The variation of amplitude a_2 via its corresponding phase γ_2: **a** when $c_1 = (0.5, 0.05, 0.005)$, **b** at $c_2 = (0.3, 0.03, 0.003)$, **c** when $\omega_2 = (0.467, 0.572, 0.808)$ at $\tau \in [0, 500]$
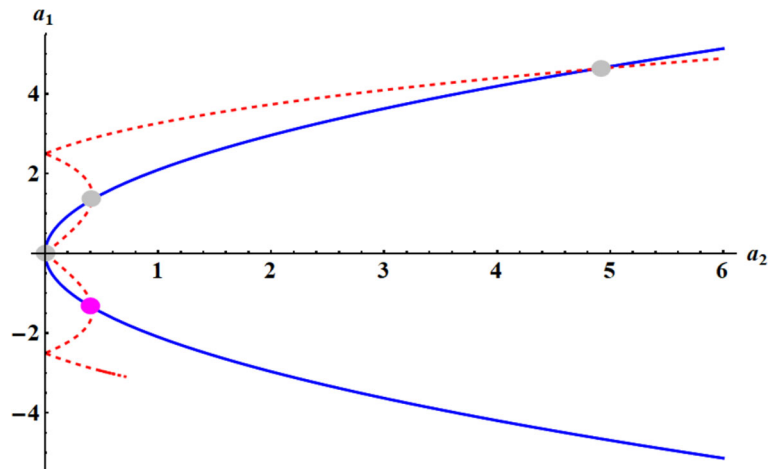
Fig. 16 Four intersection fixed points of the amplitudes a_1 and a_2 at $c_1 = 0.5$, $\omega_2 = 0.467$, and $c_2 = 0.3$
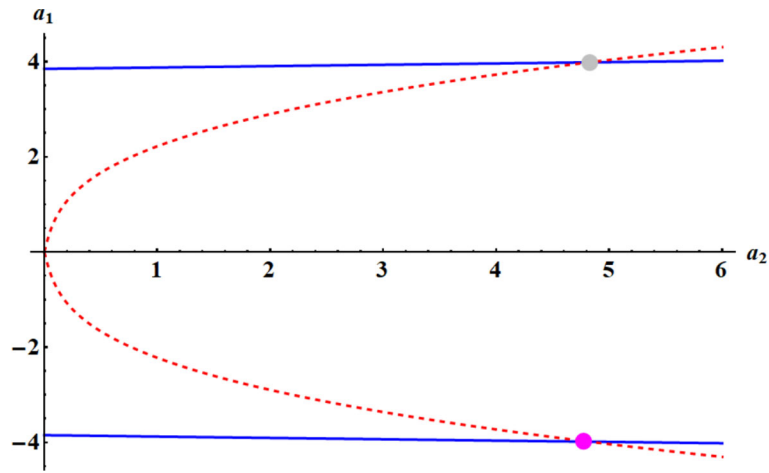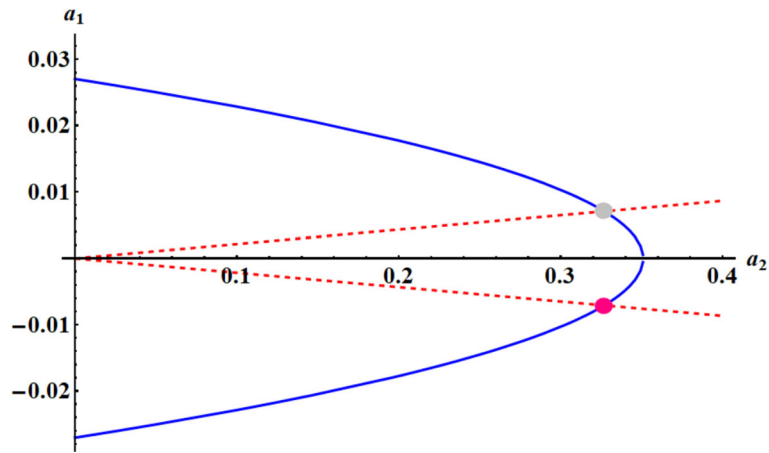
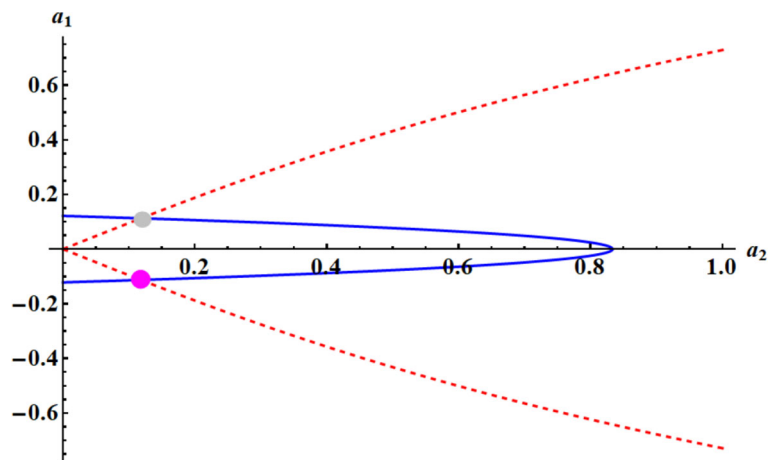**Fig. 17** Two intersection fixed points of the amplitudes a_1 and a_2 at $c_1 = 0.05$, $\omega_2 = 0.467$, and $c_2 = 0.3$

Fig. 18 Two intersection fixed points of the amplitudes a_1 and a_2 at $c_2 = 0.03, c_1 = 0.5$, and $\omega_2 = 0.467$

Fig. 19 Four intersection fixed points of the amplitudes a_1 and a_2 at $\omega_2 = 0.572, c_1 = 0.5$, and $c_2 = 0.3$
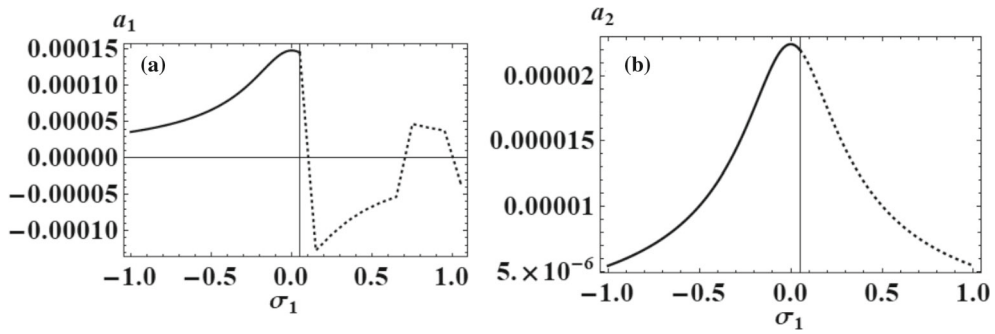
Fig. 20 The frequency response when $c_1 = 0.5$
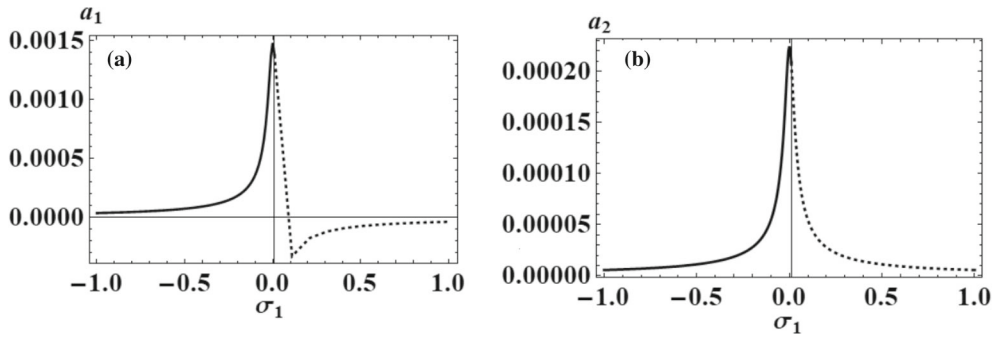
Fig. 21 The frequency response when $c_1 = 0.05$
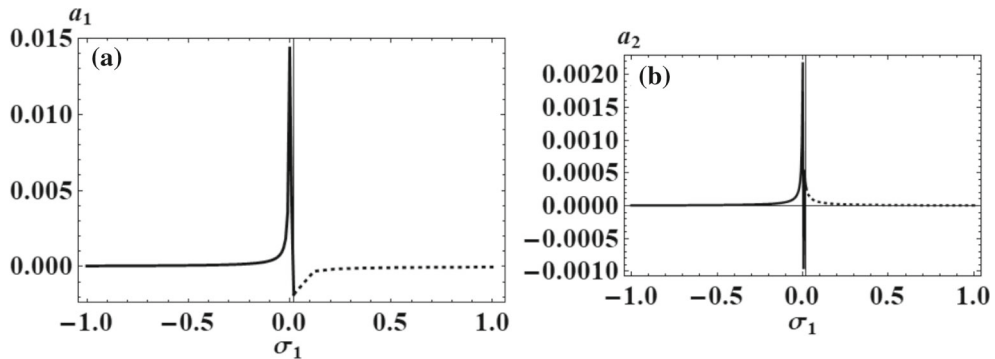
Fig. 22 The frequency response when $c_1 = 0.005$
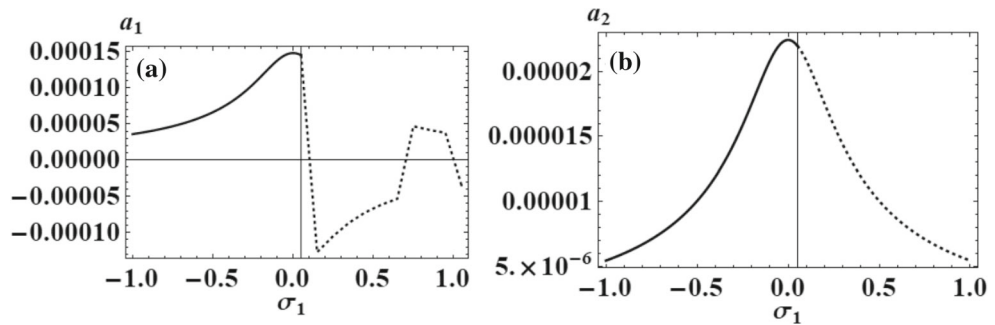
Fig. 23 The frequency response when $c_2 = 0.03$
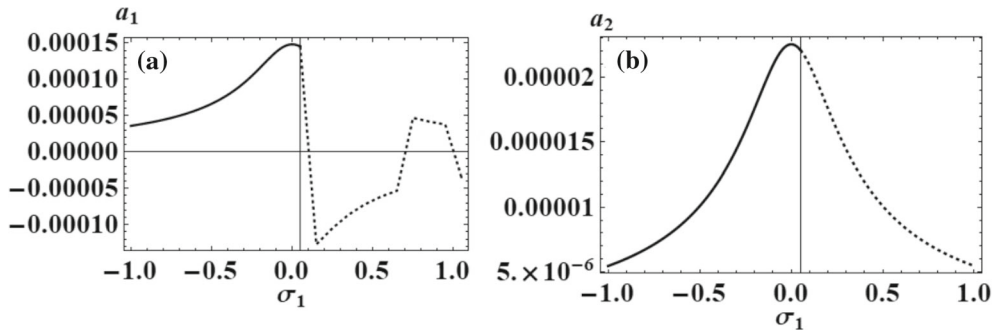
Fig. 24 Frequency response when $c_2 = 0.003$
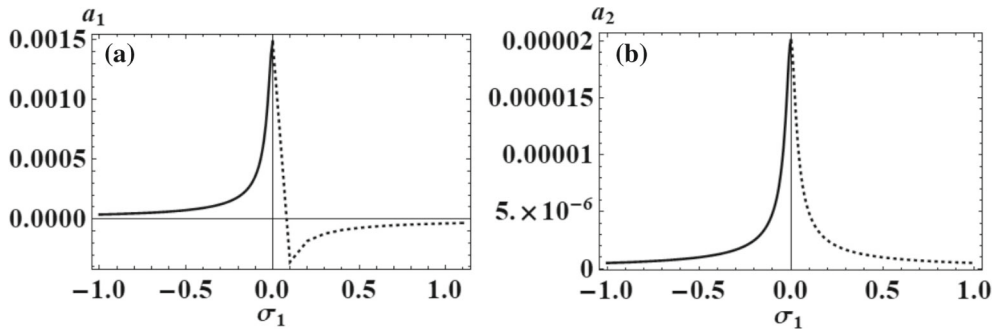
Fig. 25 Frequency response when $\omega_2 = 0.467$
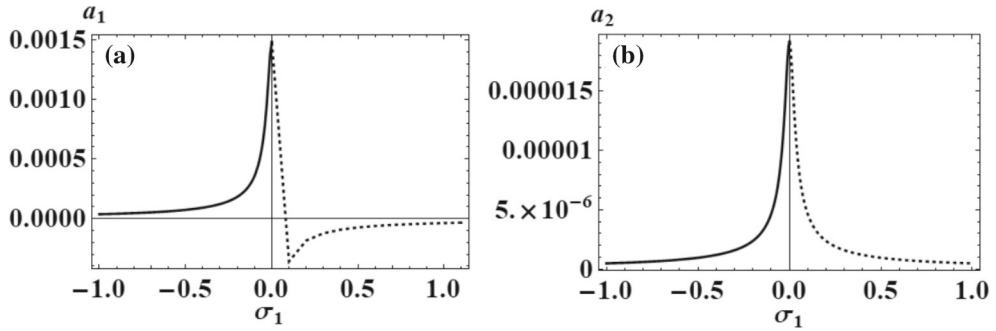
Fig. 26 Frequency response when $\omega_2 = 0.572$
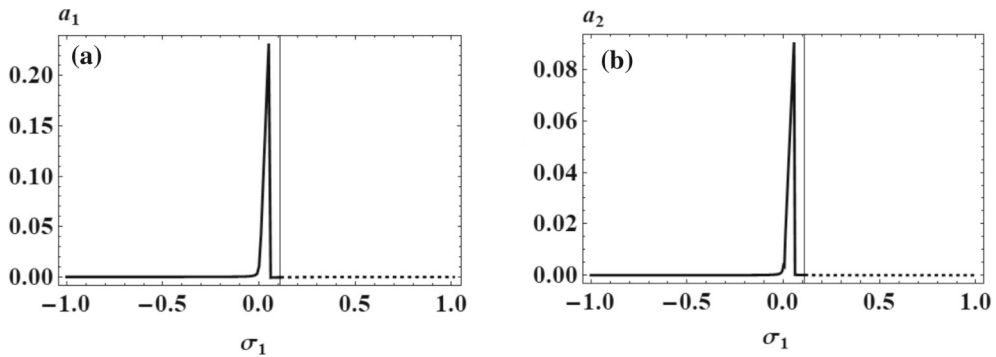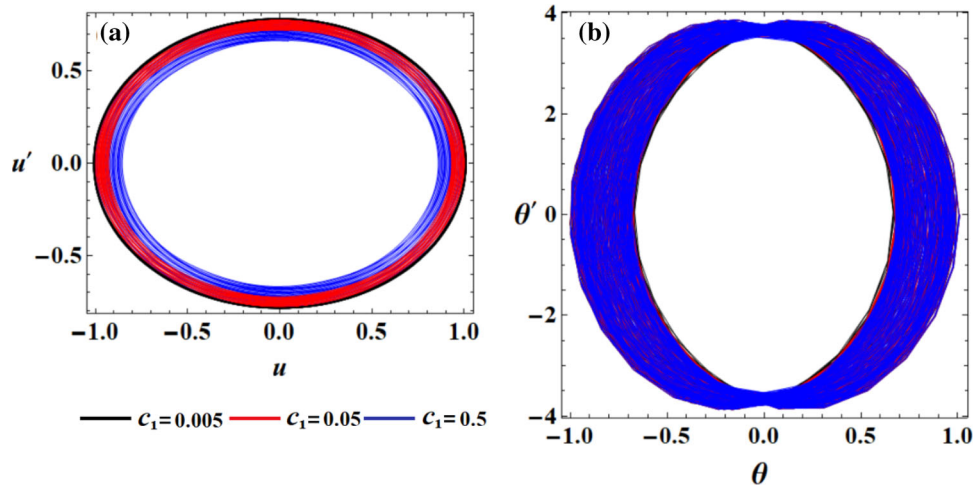

Fig. 27 The frequency response when $\sigma_2 = 0.11$

Fig. 28 The modulation equations projection at $c_1 = (0.5, 0.05, 0.005)$: **a** regarding the plane $u\,u'$, **b** regarding the plane $\theta\,\theta'$
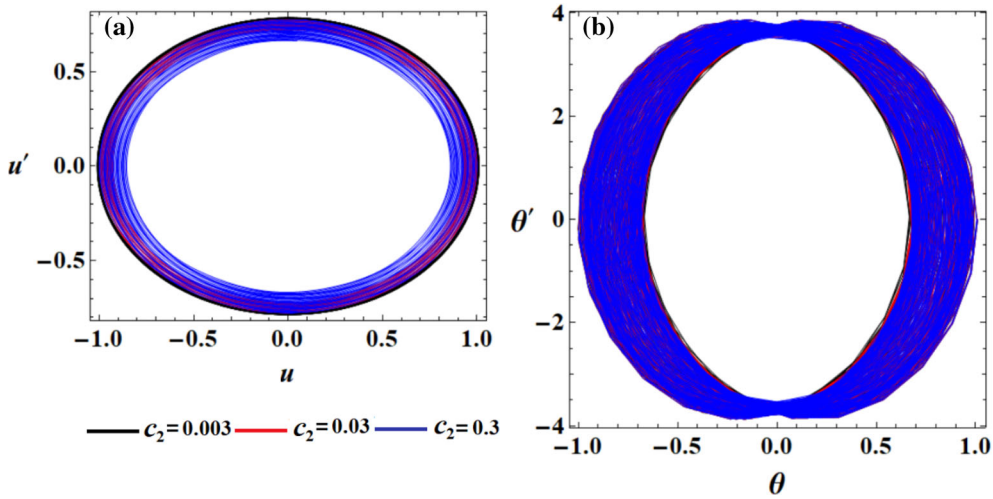

Fig. 29 The modulation equations projection at $c_2 = (0.3, 0.03, 0.003)$: **a** and **b** regarding the planes $u\,u'$ and $\theta\,\theta'$, respectively
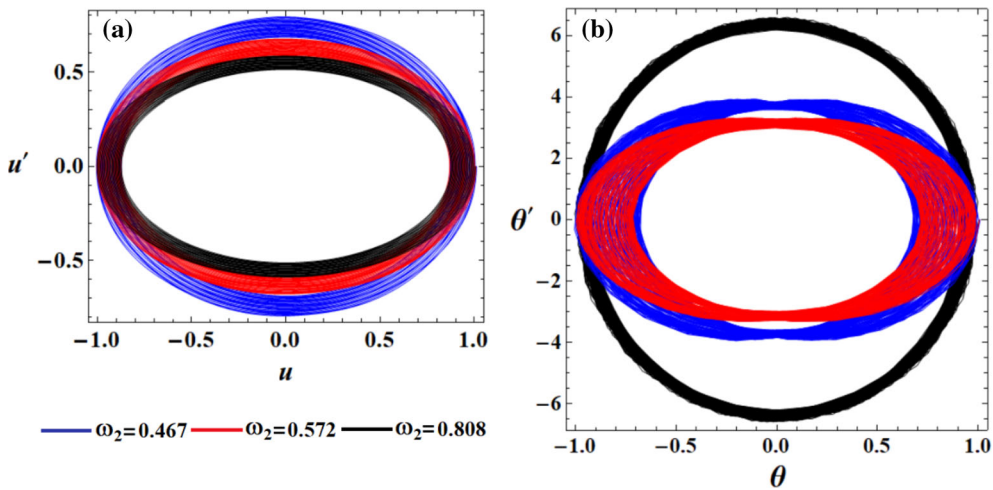

Fig. 30 The modulation equations projection at $\omega_2 = (0.467, 0.572, 0.808)$: **a** and **b** regarding the planes $u\,u'$ and $\theta\,\theta'$, respectively
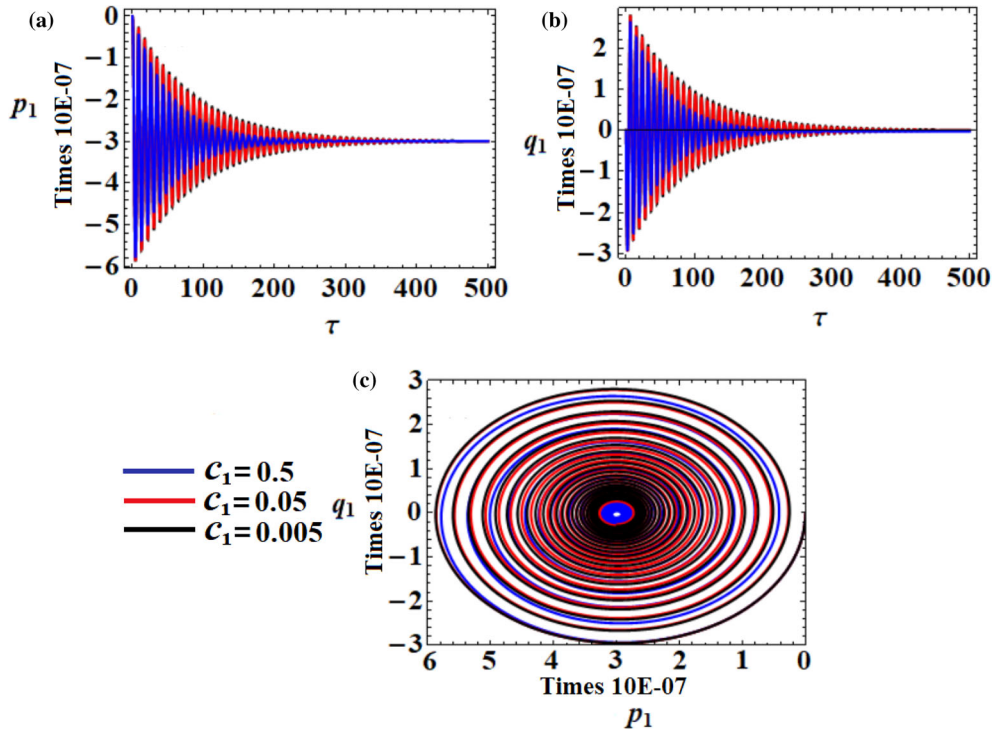
Fig. 31 a and **b** describe the variation p_1 and q_1 versus τ at $c_1(= 0.5, 0.05, 0.005)$, (c) explores the trajectories' projection of the modulation equations on p_1q_1 at the same values of c_1

$$2\omega_2 q_2' = \frac{h\,d\omega_2^4}{\omega_1^2 - \omega_2^2}p_2 - 2c_2\omega_2 q_2 + \frac{2h\,\omega_1}{\omega_2^2 - \omega_1^2}q_2 - 2\omega_2 p_2\sigma_2 - 2\omega_2^2(p_2^3 + q_2^2 p_2),$$

$$2\omega_2 p_2' = 2\omega_2 q_2\sigma_2 - \frac{h\,d\omega_2^4}{\omega_1^2 - \omega_2^2}q_2 - 2c_2\omega_2 p_2 + \frac{2h\,\omega_1}{\omega_2^2 - \omega_1^2}p_2 + 2\omega_2^2(q_2^3 + p_2^2 q_2). \qquad (41)$$

The adjusted amplitudes are then tweaked in various parameter areas throughout time, and the attributes of the amplitudes are displayed in phase diagram curves, as drawn in Figs. 31, 32 and 33 taking into account the next chosen data

$$f_1 = 0.0001, \quad \sigma_2 = 0.05, \quad \varepsilon = 0.005, \quad c_1(= 0.5, 0.05, 0.005),$$
$$c_2(= 0.3, 0.03, 0.003), \quad \omega_1(= 0.467, 0.572, 0.808).$$

Figure 31 depicts the modified phases' variation p_1 and q_1 overtime τ and the projection of the modulation equation's route on the phase plane p_1q_1 at various values of c_1. Parts (a) and (b) have decay curves, while spiral curves are drawn on part (c). Then, one can conclude that the dynamical behavior of the above system of Eq. (41) has a stable manner, in which the transformations (40) are used. The influence of different values of c_2 on the system's behavior has a slight effect, as seen in Fig. 32, which is due to the formulations of Eqs. (41). On the other hand, the good impact of the frequency values is evident from the plotted curves in Fig. 33. The changed amplitudes decrease with time, eventually approaching zero, as can be seen in Figs. 31, 32 and 33. The spiral's path, among several other things, is a significant indicator of the stationary behavior of the dynamical systems.

6 Conclusion

The motion of a 2DOF auto-parametric dynamical system consisting of a linked rolling cylinder with a damped spring has been studied. This motion has been considered under the influence of an excitation force. The guiding system of motion has been constructed using Lagrange's equations and has been solved using the TMS up
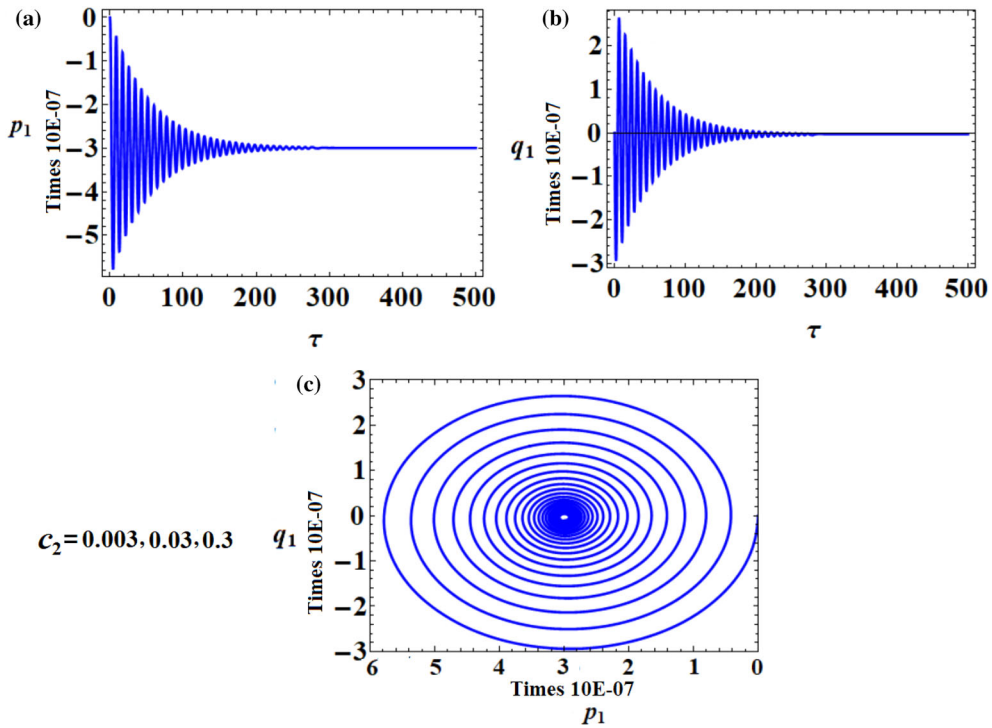
Fig. 32 **a** and **b** describe the variation p_1 and q_1 versus τ at $c_2(= 0.003, 0.03, 0.3)$, (**c**) explores the trajectories' projection of the modulation equations on $p_1 q_1$ at the same values of c_2
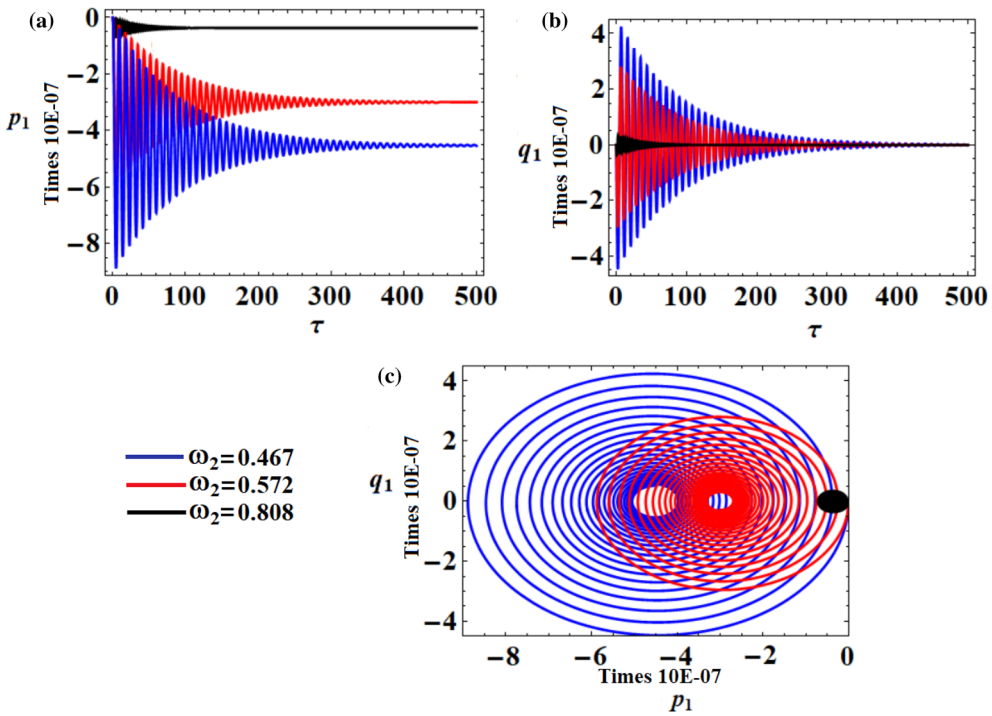

Fig. 33 **a** and **b** describe the variation p_1 and q_1 versus τ at $\omega_2(= 0.467, 0.572, 0.808)$, **c** explores the trajectories' projection of the modulation equations on $p_1 q_1$ at the same values of ω_2

to third order of approximation. The equations of modulation have been constructed in the framework of the conditions of solvability. The primary external and internal resonances have been examined simultaneously. Routh–Hurwitz criteria have been utilized to examine the arising fixed points of the system at the steady state, and the stability analysis, in view of the stability and instability zones, has been investigated. The temporal variations of the amplitudes, modified phases, and obtained solutions have been drawn in a few specific plots to indicate the influence of the system's parameters on the motion. Moreover, the properties of nonlinear amplitudes of the equations of modulation have been examined and reported, as well as their stabilities. The obtained results are considered novel and original since the applied methodology is employed on a specific dynamical system. This work is significant because it has immediate applications in the disciplines of engineering machines like reducing the harmful vibrations in machines, tall buildings, chimneys, bridges, television towers, and antennas.

Data availability As no datasets were generated or processed during the current study, data sharing was not applicable to this paper.

Declarations

Conflict of interest The author has declared no conflicts of interest.

References

1. Lee, W.K., Park, H.D.: Chaotic dynamics of a harmonically excited spring-pendulum system with internal resonance. Nonlinear Dyn. **14**, 211–229 (1997)
2. Lee, W.K., Park, H.D.: Second-order approximation for chaotic responses of a harmonically excited spring-pendulum system. Int. J. Nonlin. Mech. **34**, 749–757 (1999)
3. Amer, T.S., Bek, M.A.: Chaotic responses of a harmonically excited spring pendulum moving in circular path. Nonlinear Anal. Real World Appl. **10**, 3196–3202 (2009)
4. Amer, T.S., Bek, M.A., Hamada, I.S.: On the motion of harmonically excited spring pendulum in elliptic path near resonances. Adv. Math. Phys. **2016**, 1–15 (2016)
5. Amer, T.S., Amer, W.S.: A study on the dynamical behavior of a rigid body suspended on an elastic spring. J. Comput. Theor. Nanosci. **14**, 1163–1167 (2017)
6. Amer, T.S.: The dynamical behavior of a rigid body relative equilibrium position. Adv. Math. Phys. **2017**, 1–13 (2017)
7. Tondl, A., Nabergoj, R.: Dynamic absorbers for an externally excited pendulum. J. Sound Vib. **234**(4), 611–624 (2000)
8. Zhu, S.J., Zheng, Y.F., Fu, Y.M.: Analysis of non-linear dynamics of a two-degree-of-freedom vibration system with nonlinear damping and non-linear spring. J. Sound Vib. **271**, 15–24 (2004)
9. Weibel, S., Kaper, T., Baillieul, J.: Global dynamics of a rapidly forced cart and pendulum. Nonlinear Dyn. **13**, 131–170 (1997)
10. Amer, W.S., Amer, T.S., Starosta, R., Bek, M.A.: Resonance in the cart-pendulum system-an asymptotic approach. Appl. Sci. **11**(23), 11567 (2021)
11. Nayfeh, A.H.: Introduction to Perturbation Techniques. Wiley, Hoboken (2011)
12. Strogatz, S.H.: Nonlinear Dynamics and Chaos: With Applications to Physics, Biology, Chemistry, and Engineering, 2nd edn. Princeton University Press, Princeton (2015)
13. Awrejcewicz, J., Starosta, R., Sypniewska-Kamińska, G.: Asymptotic Multiple Scale Method in Time Domain Multi-Degree-of-Freedom Stationary and Nonstationary Dynamics. CRC Press, Boca Raton (2022)
14. Starosta, R., Sypniewska-Kamińska, G., Awrejcewicz, J.: Parametric and external resonances in kinematically and externally excited nonlinear spring pendulum. Int. J. Bifurcat. Chaos **21**(10), 3013–3021 (2011)
15. Starosta, R., Sypniewska-Kamińska, G., Awrejcewicz, J.: Asymptotic analysis of kinematically excited dynamical systems near resonances. Nonlinear Dyn. **68**(4), 459–469 (2012)
16. Amer, T.S., Bek, M.A., Abouhmr, M.K.: On the vibrational analysis for the motion of a harmonically damped rigid body pendulum. Nonlinear Dyn. **91**, 2485–2502 (2018)

17. Amer, T.S., Bek, M.A., Abouhmr, M.K.: On the motion of a harmonically excited damped spring pendulum in an elliptic path. Mech. Res. Commu. **95**, 23–34 (2019)
18. El-Sabaa, F.M., Amer, T.S., Gad, H.M., Bek, M.A.: On the motion of a damped rigid body near resonances under the influence of harmonically external force and moments. Results Phys. **19**, 103352 (2020)
19. El-Sabaa, F.M., Amer, T.S., Sallam, A.A., Abady, I.M.: Modeling and analysis of the nonlinear rotatory motion of an electromagnetic gyrostat. Alex. Eng. J. **61**(2), 1625–1641 (2022)
20. Salahshoor, E., Ebrahimi, S., Maasoomi, M.: Nonlinear vibration analysis of mechanical systems with multiple joint clearances using the method of multiple scales. Mech. Mach. Theory **105**, 495–509 (2016)
21. Plakhtienko, N.P., Mikhailova, M.I., Zabuga, A.T.: Vibrations of a rigid body with a controlled frictional electromagnetic seismic damper, nonlinear model. Int. Appl. Mech. **46**(1), 103–112 (2010)
22. Legeza, V.: Dynamics of vibration isolation system with a quasi-isochronous roller shock absorber. Int. Appl. Mech. **47**(3), 329–337 (2011)
23. Sado, D., Gajos, K.: Analysis of vibration of three degree-of-freedom dynamical system with double pendulum. J. Theor. Appl. Mech. Pol. **46**, 141–156 (2008)
24. Amer, T.S., Starosta, R., Almahalawy, A., Elameer, A.S.: The stability analysis of a vibrating auto-parametric dynamical system near resonance. Appl. Sci. **12**, 1737 (2022)
25. He, J.-H., Amer, T.S., Abolila, A.F., Galal, A.A.: Stability of three degrees-of-freedom auto-parametric system. Alex. Eng. J. **61**(11), 8393–8415 (2022)
26. Sartorelli, J.C., Lacarbonara, W.: Parametric resonances in a base-excited double pendulum. Nonlinear Dyn. **69**, 1679–1692 (2012)
27. Sypniewska-Kamińska, G., Awrejcewicz, J., Kamiński, H., Salamon, R.: Resonance study of spring pendulum based on asymptotic solutions with polynomial approximation in quadratic means. Meccanica **56**, 963–980 (2021)
28. Bek, M.A., Amer, T.S., Abohamer, M.K.: On the vibrational analysis for the motion of a rotating cylinder. In: Awrejcewicz, J. (Ed) Perspectives in Dynamical Systems I: Mechatronics and Life Sciences. DSTA 2019. Springer Proceedings in Mathematics & Statistics, vol. 362, pp. 1–15 (2022)
29. Nayfeh, A.H., Mook, D.T.: Nonlinear Oscillations. WILEY-VCH Verlag GmbH & Co, KGaA (2004)
30. Abdelhfeez, S.A., Amer, T.S., Elbaz, R.F., Bek, M.A.: Studying the influence of external torques on the dynamical motion and the stability of a 3DOF dynamic system. Alex. Eng. J. **61**, 6695–6724 (2022)
31. Amer, W.S., Amer, T.S., Hassan, S.S.: Modeling and stability analysis for the vibrating motion of three degrees-of-freedom dynamical system near resonance. Appl. Sci. **11**(24), 11943 (2021)
32. Bek, M.A., Amer, T.S., Sirwah, M.A., Awrejcewicz, J., Arab, A.A.: The vibrational motion of a spring pendulum in a fluid flow. Results Phys. **19**, 103465 (2020)
33. Amer, T.S., Starosta, R., Elameer, A.S., Bek, M.A.: Analyzing the stability for the motion of an unstretched double pendulum near resonance. Appl. Sci. **11**, 9520 (2021)
34. Amer, T.S., Bek, M.A., Hassan, S.S.: Sherif Elbendary, The stability analysis for the motion of a nonlinear damped vibrating dynamical system with three-degrees-of-freedom. Results Phys. **28**, 104561 (2021)
35. Amer, T.S., Galal, A.A., Abolila, A.F.: On the motion of a triple pendulum system under the influence of excitation force and torque. Kuwait J. Sci. **48**(4), 1–17 (2021)
36. Bek, M.A., Amer, T.S., Almahalawy, A., Elameer, A.S.: The asymptotic analysis for the motion of 3DOF dynamical system close to resonances. Alex. Eng. J. **60**, 3539–3551 (2021)
37. Amer, T.S., Bek, M.A., Hassan, S.S.: The dynamical analysis for the motion of a harmonically two degrees of freedom damped spring pendulum in an elliptic trajectory. Alex. Eng. J. **61**(2), 1715–1733 (2022)